The Impact of Surface Structure on Laser Triggered Electrical Breakdown

Master Thesis
by
Dan Liungman

Lund Reports on Atomic Physics, LRAP-222
Lund, September 1997

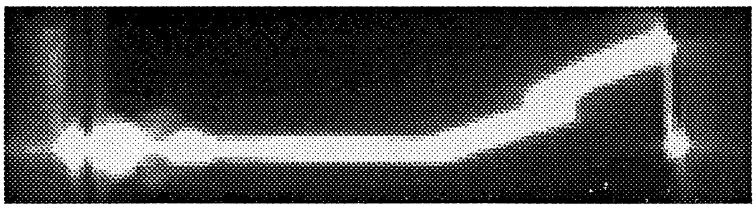

Supervisors:
Anders Sunesson
Mikael Bergkvist

Examiner:
Stefan Kröll

This thesis was submitted to the
Faculty of Technology at Lund University
in partial fulfilment of the requirements for
the degree of Master of Science.

Abstract

By firing a laser pulse onto the surface of one of the electrodes in a high-voltage spark gap, it is possible to reduce the voltage at which breakdown will occur. This is called laser triggered breakdown. It is also possible to control the breakdown in time. The impact of changing the absorptance by altering the surface structure of the electrode was investigated regarding parameters such as breakdown voltage, delay time and reliability. It was shown that within certain limits e.g. homogeneity of the electric field, the surface structure and the absorptance has little or no effect on the breakdown characteristics. Furthermore it was shown that moving the laser focus out from the surface changes the breakdown voltage dramatically, and that the polarity of the struck electrode is of importance to the process. The laser used was a Nd:YAG (1064 nm) and the electrode material was aluminium.

Table of Contents

1. Introduction

Laser triggering is a method of controlling electrical breakdowns. It is done by increasing the charge density in the gap exposed to the electrical field, usually through the creation of a plasma (or several) in the gap. The plasma can either be created somewhere in the insulating medium between the electrodes or on the surface of one of them.
A spark gap (Appendix A, figure 40) is an electrical device in which two electrodes are separated by a gap of insulating medium. Sufficient voltage over the gap causes it to collapse, i.e. a bright, conducting plasma channel (breakdown arc) bridges the gap, thereby closing it.
The technique of triggering spark gaps with lasers has been studied and tested for over thirty years. There are several known applications ranging from the timing of the ignition in spark plugs for cars, through high-voltage switchgear for ion-beam fusion drivers, to the triggering of lightnings to prevent sensitive high-voltage installations from being struck during thunderstorms (Figure 1).

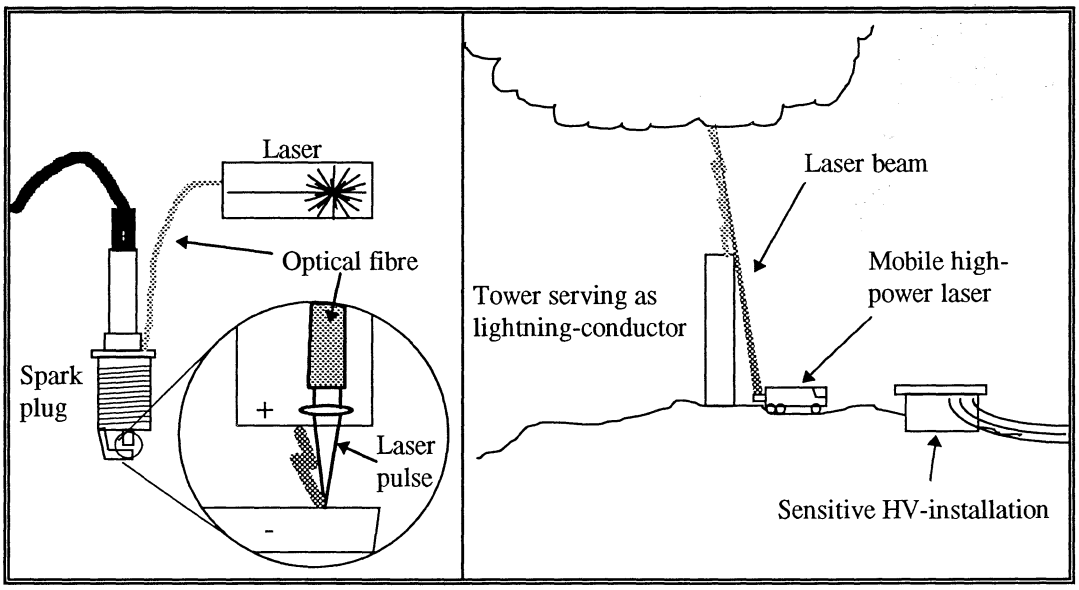

Figure 1. Laser triggering on different scales.

Although the phenomena has been studied so thoroughly it is far from fully understood. The reason for this is probably the combination of the two complicated fields: interaction between laser light and matter, and breakdown/plasma physics.

1.1. AIM AND COMPOSITION

In surface triggering one of the electrodes is the target for the triggering laser pulse. The aim of this project has been to investigate the consequences of changing the structure of this surface. With a rougher surface and higher absorption at the laser wavelength the idea was that the pulse energy required to trigger a gap at a specific voltage would drop. Another purpose with the project was to investigate methods of characterising the electrode surfaces.

The composition of this report is almost chronological. It begins with the manufacturing and processing of the samples done by me and the workshop at ABB Corporate Research in April 1997. Then it deals with the characterisation of the surfaces done by myself at the Ångström Laboratory in Uppsala the following month. The last sections are about the actual breakdown experiments performed at Lund Institute of Technology during the summer.

1.2. BACKGROUND

Pendleton and Guenther [1] made their first experiments on laser triggering in 1965. Since then an extensive amount of work has been done on the subject, mostly of an engineering rather than physical character. In the United States a lot of projects have had connections to the fusion research programs [2] there since that is an area where quick, reliable, very high power switching is crucial. Research on using laser triggering to control lightnings is almost exclusively performed in Japan where thunderstorms are a major problem to the power industry.

Most of the research and development today focus on improving the characteristics of the triggered breakdowns. These include the laser power required for triggering, the delay time between triggering and breakdown, the maximum current through the gap, the time it takes for the current to reach the desired level and the reliability of the systems. These improvements are made by altering the following parameters:

- Surface or volume triggering (4.1.2).
- Insulating medium between the electrodes, e.g. oil, water, gas, air etc.
- Pressure of the medium.
- Geometry of the gap.
- Triggering laser wavelength.
- Polarity of the gap.

Not much have been published on the effect of changing the surface structure of the electrode however, making this project the more interesting.

2. Sample Manufacturing and Processing

2.1. SAMPLE MANUFACTURING

Since the aim of the project was to study the effect of various electrode surface structures on laser triggered breakdowns, the most natural thing to do might have been to manufacture a couple of electrodes, each with a slightly different surface structure. However, due to high demands on the homogeneity of the electric field and in order to avoid glow discharges the electrodes have to be fairly large and of a quite complicated shape (Appendix A, figure 40), [3]. It was therefore decided to fabricate several small samples that could be placed one by one in a hole on the electrode. This also facilitated the processing and the characterisation of the surfaces.

The samples had to fulfil the following requirements:

- They were to be used with one of the existing electrodes.
- They had to be easily changeable.
- They had to be adjustable as to assure a homogeneous electric field.
- They had to be small enough to fit into the characterisation equipment.

These conditions resulted in a 50 x 5mm (diameter x thickness) disc with a 18 x 25 mm bolt on one side (Figure 2). The samples were made from a solid piece of aluminium.

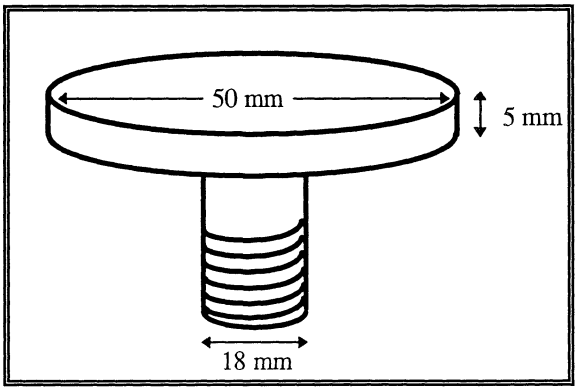

Figure 2. A sample at approximately real size.

The central part of the electrode was removed to fit the sample.
Twenty-four samples like this were made at the workshop at ABB Corporate Research in Västerås. Their top surfaces were then processed to different structures and roughness through etching, sand-blasting, grinding and polishing. All except two were grinded to remove traces of turning. Ten samples were then blasted, five were etched, five were further grinded and two were polished. The remaining two were left untouched.

2.2. ETCHING

Etching was done by myself in the chemical laboratory at the Department of Solid State Physics, Ångström Laboratory in Uppsala. It was made by dipping the samples into strong solutions of sodium hydroxide. In order to protect the rest of the sample from damage, only the top surface was dipped. An unforeseen problem at this stage was that the hydrogen gas produced by the chemical reaction formed large bubbles that disturbed the process, making it difficult to evaluate the results of different etching times and concentrations. This should not be a problem in future applications however, since there exist standard industrial procedures for etching aluminium. Another problem was the deposition of aluminium hydroxide causing dark spots on the surface.

2.3. SAND-BLASTING

Sand-blasting was done by myself in the workshop of the Ångström Laboratory. A closed industrial blaster was used with glass-sand (GL-6). The samples were held by hand for different lengths of time, at different angles and at different distances from the nozzle. The main problem here was to get an even blasting over the whole surface. This was done by moving the sample around under the nozzle.

2.4. GRINDING AND POLISHING

The grinding and polishing was done with a Buehler Ecomet 2. For grinding I used Struers grinding paper of grit 500 to 4000 and for polishing I used polishing cloth with 2 μm (diamond) polishing fluid. Polishing in this way was very difficult. Sometimes it was just impossible to get a good result and a small mistake could easily spoil an hour's work.

2.5. SUMMARY

Due to the fact that the original samples were too big to fit in all the instruments I decided to arrange them in pairs. I processed the two surfaces in each pair identically and then cut off the bolt on one sample in each pair. This gave me the following set of samples (Table 1):

Sample	Bolt	Surface processing	Comment
1	x	Polished	Smoth and shiny, visible
23		Polished	marks from polishing.
2	x	Grinded	Very smooth but not
13		Grinded	shiny.
12		Grinded	Clear marks from
14	x	Grinded	grinding (anisotropic).
3	x	Turned	No processing at all.
10		Turned	Clear circular pattern from turning.
6		Etched	Quite smooth, very
8	x	Etched	white.
11	x	Etched	Like 6 & 8, + tiny holes.
9	x	Etched	Rough, deep "worm
7		Etched	holes".
4		Blasted	10 sec. 10 cm from
5	x	Blasted	nozzle, normal incidence. Dark.
15	x	Blasted	20 sec. 40 cm from
16		Blasted	nozzle, normal incidence. Rough but shiny.
17	x	Blasted	20 sec. 20 cm from
18		Blasted	nozzle, normal incidence. Like 15/16, little darker.
19	x	Blasted	60 sec. 10 cm from
20		Blasted	nozzle, 45 incidence. Waves, anisotropic. Like "fingerprint".
21		Blasted	60 sec. 10 cm from
22	x	Blasted	nozzle, normal incidence. Quite smooth, dark.
24	x	Polished	very smooth and shiny, no marks.

Table 1. Samples.

3. Sample Characterisation

The following section deals with surface characterisation procedures performed at the Ångström Laboratory in Uppsala. It begins with a general description of the concept of surface characterisation. Chapter 3.2 introduces Surface Roughness while 3.3 and 3.4 describe ways to measure it. Chapter 3.5 and 3.6 are about the instrument used for this project, the measuring procedures and the results of the surface characterisation.

3.1. SURFACE CHARACTERISATION

In order to compare the breakdown properties of different surfaces it is necessary to characterise the surfaces used for the experiment. All samples were of the same aluminium material wherefore the main quantity for characterisation became the surface structure or surface roughness. Since the absorption of laser energy in the surface was thought to be of great importance for the triggering mechanism, the total absorptance at the triggering laser (Nd:YAG) wavelength (1064 nm) was also considered an interesting quantity to investigate. Increasing the absorption by using anti-reflecting coating was however not included in this project.

Important parameters for characterising the surfaces:

- Surface roughness
- Absorptance at 1060 nm

3.2. SURFACE ROUGHNESS

Imagine a big empty parking lot. Then imagine a large iceberg next to it. Now tell me which is rougher. Looking from a distance you will probably find the flat parking lot smoother than the rugged iceberg, but looking more closely, the smooth sides of the iceberg will appear perfectly flat compared to the rugged tar surface of the parking lot. It is obviously necessary to define the scale before it is possible to compare the roughness of two surfaces. This makes characterisation of surface roughness a complicated matter. In my case there are fairly well defined limits to the scale of the roughness. The surface of the sample has to be flat enough to keep the electric field homogenous and to avoid discharges from macroscopic bumps on the surface. The lower limit is that the laser pulse is unaffected by structures significantly smaller than the wavelength of the light. This still leaves me with a range of approximately 10 nm - 100 mm or a factor of 10 000.
Surface roughness can be measured directly by an instrument that gives the surface profile, or it can be calculated from measurements of scattering from the surface.

3.2.1. Roughness Quantities

Many physical quantities, like length and weight, are unambiguous. Roughness however is not. It can be defined and measured in many different ways. The most common will be explained below:

- *Rms*-roughness or δ (unit: m)

(1) $$\delta = \sqrt{\frac{1}{N} \cdot \sum_{i=1}^{N} z_i^2}$$

Where: N is the number of discrete, equally spaced measured points.
z_i is the distance of point i from the mean surface level.

- *Ra* or average roughness (unit: m)

(2) $$R_a = \frac{1}{N} \cdot \sum_{i=1}^{N} |z_i|$$

Note that the only difference between δ and R_a is the square on the height (z_i). The consequence of this is that the two quantities are almost equal for surfaces with only small deviations from the average level while δ becomes significantly larger for surfaces with deep holes or big bumps.

- *Rms*-slope

Defined as δ but with m_i instead of z_i, where m_i is the angle of the line between point i and point i+1 approximated according to:

(3) $$m_i = \frac{(z_{i+1} - z_i)}{\tau_0}$$

t_0 is the sampling interval or the distance between the points measured along the mean surface level.
Rms-slope is a complement to the *rms*-roughness. It can for example be used to distinguish between two sinusoidal surfaces with different spatial wavelength but equal amplitude and therefore equal *rms*-roughness.

- Power Spectral Density function or *PSD*-function (unit: m^{-1})

The square of the Fourier transform of the surface profile, i.e. the frequency spectrum of the surface roughness.
The *PSD*-function indicates if there are any anisotropies or regularities in the surface profile. This is often the case with mechanically produced surfaces where the tools make regular scratches. Etching and sand-blasting do not normally produce such regularities but by tilting the sample while sand-blasting, a wavy pattern was made on the surface much like sand dunes in the dessert.

Rms-roughness and R_a were the most important quantities used in this project as they were the quantities given by several of the instruments. Note that different instruments will give different values of surface roughness depending on their bandwidth.

3.3. MEASURING SURFACE ROUGHNESS WITH PROFILERS

Instruments directly measuring the surface profile can be divided into two groups: contact and non-contact instruments.
Contact instrument use a probe that follow the surface. The most common contact method is letting a sharp needle glide across the surface while measuring it's vertical movements. The range of this method is limited by the size of the stylus, the distance between the samples during the scan and the length of the scan. Naturally the needle can not fully follow the profile of the surface if the stylus is bigger than the surface structures (Figure 3). Another disadvantage is that the sharp needle can force it's way through the surface structure like the bow of a large ship through rough sea, thereby giving erroneous results and damaging the sample. This was not a problem for me using large, rather hard samples.

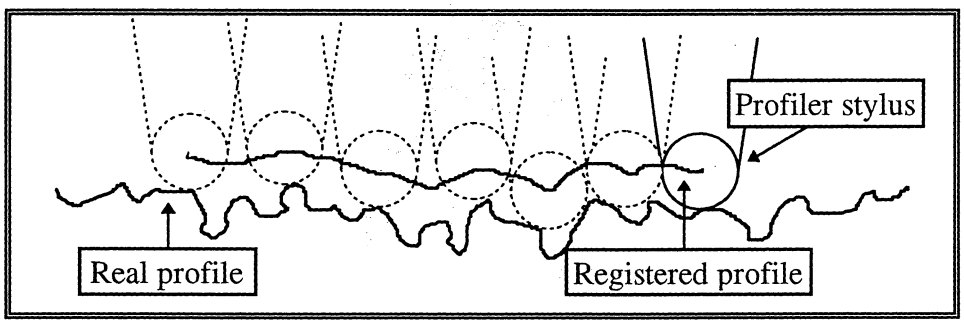

Figure 3. A profiler filters structures smaller than the size of the stylus.

Atomic Force and Tunnelling Microscopy can also be considered as contact profiling methods. None of these were used in this project though.
Most non-contact profilers use interferometry to measure the vertical position of a point on the sample. Some instruments detect changes in focus. The common feature of these is that they use light beams to obtain a surface profile. An exception is the Electron Microscope which uses electrons to make an image of the surface.

3.4. MEASURING SURFACE ROUGHNESS THROUGH SCATTERING

Under some special circumstances it is possible to determine surface roughness by making light scattering measurements. A very smooth surface (mirror) scatters or reflects an incoming light beam in one direction while a rough surface (piece of paper) scatters light diffusely in all directions. How this can be used for measuring surface roughness will be described in the following chapters.

3.4.1. Scattering

All objects scatter light in one way or another. According to Huygens-Fresnel's principle light will be scattered in the direction or directions giving constructive interference between light waves coming from different parts of the surface. This is why a flat surface scatters in the angle of reflection, a grating scatters in several specific directions and a rough surface scatters in all directions (Figure 4).

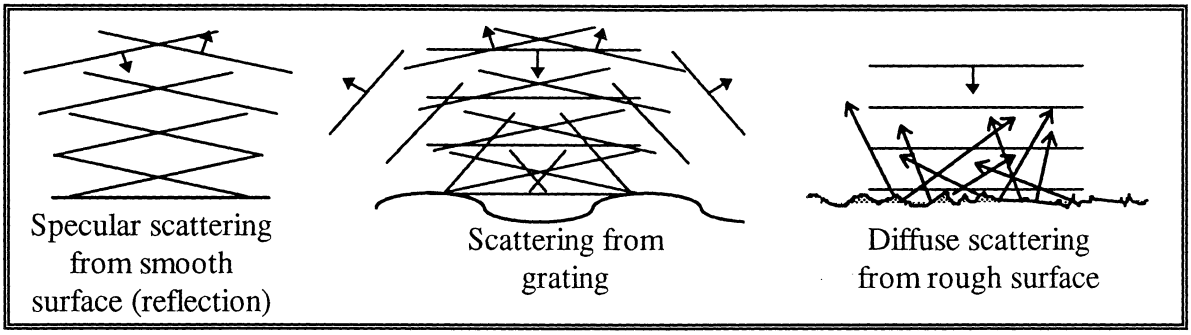

Figure 4. Scattering from different surfaces.

When we say reflection we usually mean scattering from a smooth surface in one direction (angle of reflection). This is henceforth called specular scattering while light scattered in other directions is called diffuse scattering. A surface for which you can not distinguish the specular component from the diffuse is called a Lambertian surface.

3.4.2. Measurements of Scattering

Measurements of scattering from surfaces are often divided into integrated scattering and angle-resolved scattering. The former is made by separately measuring the diffuse components of the scattered light. The diffusely scattered light is collected with an integrating sphere (Figure 11) or a focusing mirror (Coblentz sphere, figure 5) while the specular component is let out through a hole in the sphere/mirror. The total scattering is measured by covering the hole. The quantity *TIS* (Total Integrated Scattering) is defined as the ratio between the diffuse component and the total scattering (Eq. 4). *TIS* can under some circumstances be used to calculate the surface roughness (see scalar theory).

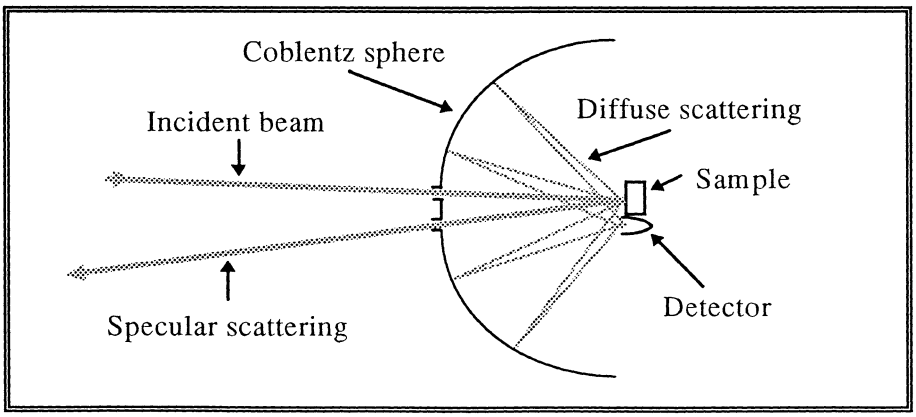

Figure 5. Measuring integrated scattering with a Coblentz sphere.

(4) $$TIS = \frac{P_d}{P_t}$$

TIS = Total Integrated Scattering
P_d = diffusely scattered power
P_t = total scattered power

If only a relative value of the roughness is needed it is possible to just calculate the ratio between the specular reflectance of the rough surfaces and that of a smooth surface.

Angle-resolved measurements are made with a detector that can be moved around the sample as if on the inside of a sphere. The sample is then illuminated with a light beam and the scattering in all different angles can be measured independently. The quantity *BRDF* (Bi-directional Reflectance Distribution Function) is defined as the ratio between the differential radiance and the differential irradiance and is a function of the two angles Θ_S and φ_S (Figure 6 and eq. 5).

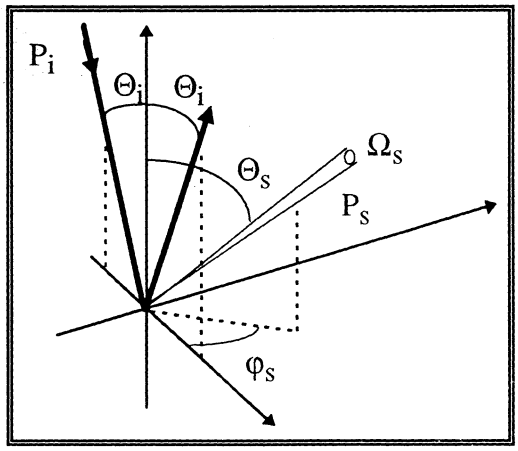

Figure 6. Definitions of *BRDF*.

(5) $$BRDF \approx \frac{dP_s / d\Omega_s}{P_i \cos\Theta_s} \approx \frac{P_s / \Omega_s}{P_i \cos\Theta_s}$$

Here, P_i is the power of the incident beam and P_S the power scattered within the solid angle Ω_S in the direction given by Θ_S and φ_S. The *BRDF* can be used to calculate the Power Spectral Density (*PSD*) function (Vector Theory, ch. 3.4.5), the square root of which is the Fourier transform of the surface profile (Eq. 6).

(6) $$F_{Fourier}\left(z_{profile}(x,y)\right) = \sqrt{PSD}$$

The *PSD* will in other words indicate the spatial wavelengths that make up the surface profile.

By integrating the *BRDF* over the hemisphere (all angles), *TIS* can be calculated and thereby also the surface roughness (Scalar Theory, chapter 3.4.4).

3.4.3. Absorptance

The total absorptance is calculated from the total scattering, measured as shown above. The reflectance is defined as the ratio between the total (specular and diffuse) scattered power and the incident power (Eq. 7).

$$R = \frac{P_{total\ scattered}}{P_{incident}} = \frac{P_{specular} + P_{diffuse}}{P_{incident}} \tag{7}$$

With the obvious assumption that no light is transmitted through the sample, the absorptance is simply given by one minus the reflectance.

3.4.4. Scalar Theory

Bennett and Porteus [4] have derived a formula relating *TIS* to the *rms*-roughness (Eq. 8), based on a scalar Kirchoff theory. *TIS* is the Total Integrated Scattering defined as in chapter 3.4.2 and the *rms*-roughness δ is defined as in chapter 3.2.1.

$$TIS = \frac{P_d}{P_t} = 1 - e^{-(4\pi\delta/\lambda)^2} \cong \left(\frac{4\pi\delta}{\lambda}\right)^2 \tag{8}$$

This so called Scalar Theory assumes that the surface is locally flat or that δ is small compared to the wavelength used for the measurement. Furthermore, the last approximation requires that $\delta << \lambda$ so that the exponential can be expanded keeping only the two first terms. This approximation was however not used in my calculations. As will be shown later, the Scalar Theory was only applicable for the smoothest of my samples.

3.4.5. Vector Theory

The surface profile, like any limited, continuos function, can be represented as a sum of sine-functions having different amplitudes, periods, phases and orientations (Figure 7).

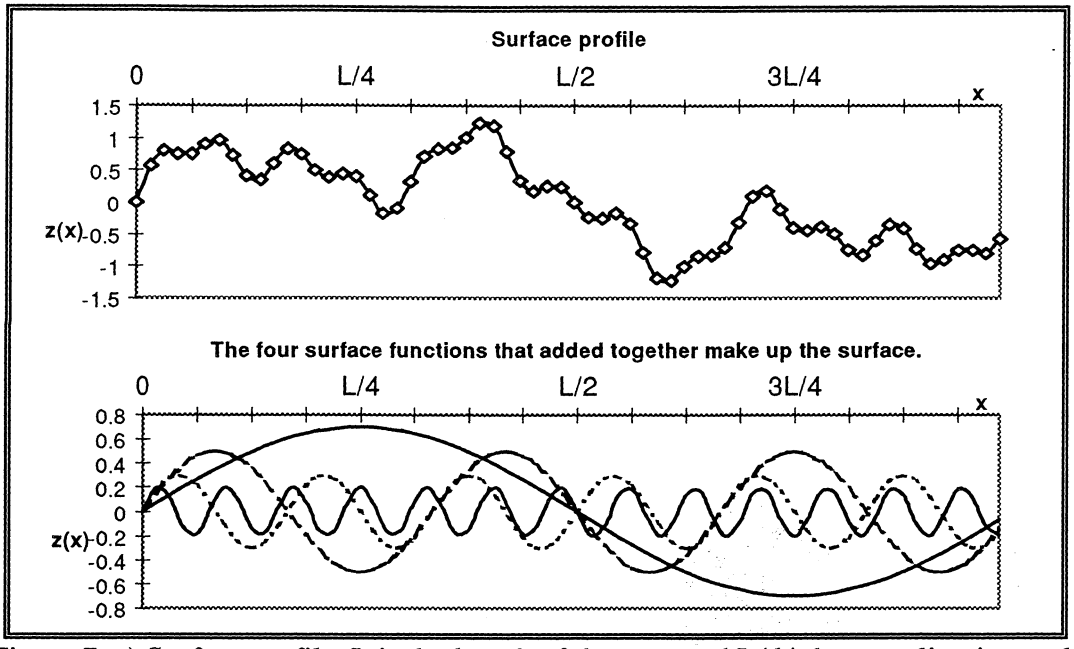

Figure 7. a) Surface profile. L is the length of the scan and L/64 the sampling interval.
b) The four components making up the Fourier transform of the profile.

The amplitudes of each of these functions are the Fourier coefficients. The spatial frequencies and the orientations define the corresponding wave-vectors. A spatial wave-vector (Figure 8) is a vector in the plane of the surface pointing perpendicularly to the waves and with a length equal to the spatial frequency.

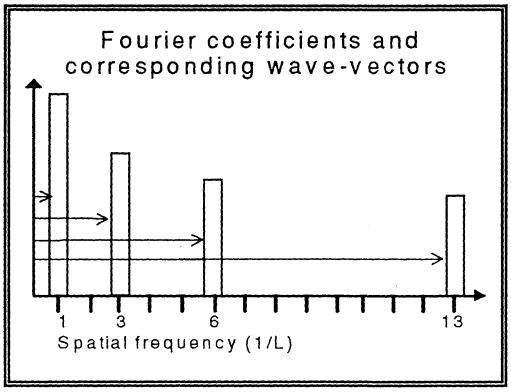

Figure 8. The amplitude of each component (Fourier coefficients).

The resolution of this way of representing a surface profile is limited by the maximum spatial frequency used in the transform. For measurements with discrete sampling, this is in turn limited to half the sampling frequency (inverse of the sampling interval).
The square of the Fourier coefficients of the surface, as a function of the wave-vectors is called the Power Spectral Density function.

The vector theories relate the scattering in a certain angle with a spatial wave-vector of the surface through the grating equation. The surface is seen as a lot of gratings with different orientations and grating indexes, and the diffuse scattering from it is simply the superposition of the diffraction patterns from each of these gratings.

Observe that spatial wavelengths shorter than the wavelength of the light do not produce any scattering and that very long spatial wavelengths produce first-order scattering very close to the angle of incidence and will thus be difficult to dissolve (Figure 9).

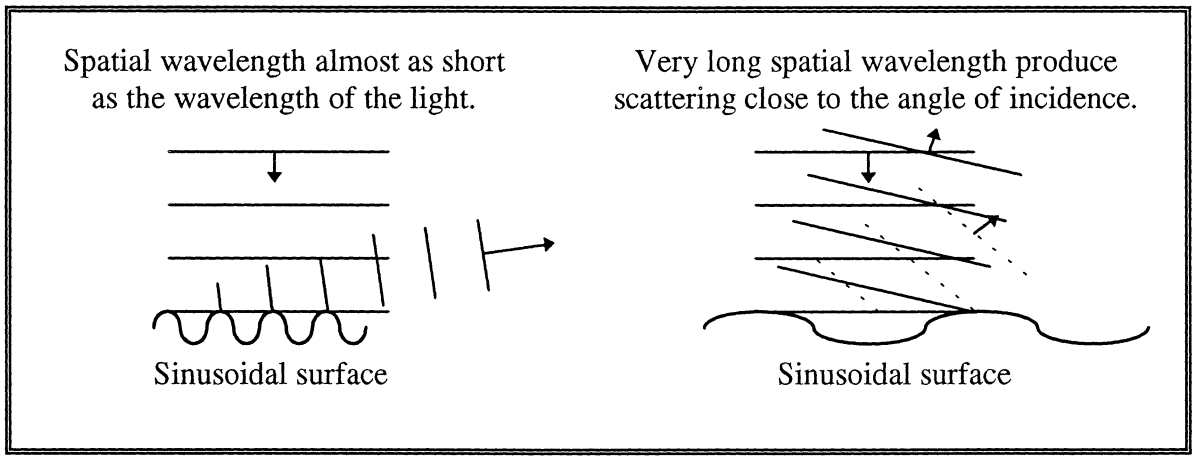

Figure 9. Scattering of light from specific spatial wavelengths.
Dotted lines show second-order diffraction.

To make calculations possible it is necessary to assume only first order diffraction (Figure 9). This requires that the *rms*-roughness of the surface is a lot smaller than the wavelength of the light (only true for my smoothest sample). The actual formula relating *BRDF* to *PSD* is rather complicated and will not be discussed here. It can however be found in any book on light scattering such as Introduction to Surface Roughness and Scattering by Bennett and Mattsson [5].

3.5. INSTRUMENTS USED FOR SURFACE CHARACTERISATION

3.5.1. WYKO

For roughness measurements on very smooth surfaces I used a WYKO Topo-3D 20 (henceforth called the WYKO). The WYKO is a non-contact micro-surface measuring system based on optical interferometry. The main components are a monochromatic light-source (tungsten halogen lamp with bandpass filter), a beam-splitter, a Mirau interferometer with a reference surface mounted on a piezoelectric translator (PZT), and a 256x256-array solid-state detector (Figure 10). The optical system is connected to an interface module with a video digitiser and the PZT-controller. The interface is then connected to a HP 320 desktop computer with which the data is analysed.

3.5.1.1.Function

Light from the tungsten halogen lamp is spectrally filtered at 650 nm with a 40 nm bandpass filter to increase the coherence of the light. The light is then reflected by a beam-splitter down towards the sample. Part of it is reflected back by a semi-transparent mirror (beam-splitter) in the Mirau interferometer on to the small reference mirror mounted on the PZT, and the rest is reflected by the sample. These two reflected beams meet again at the semi-transparent mirror and will interfere and produce a fringe pattern at the detector-array under the condition that the distance travelled by the two beams are the same (limited coherence). When making a measurement the reference mirror is moved slightly thus inducing a phase-shift or a movement of the fringe pattern. This movement is analysed by the computer and translated into a topographic profile of the sample. Of course this requires that the reference mirror is perfectly smooth.
Note that if the semi-transparent mirror is tilted 45 degrees and the reference mirror is placed at right angle beside it, we would have a Michelson interferometer.
The focusing of the system is done manually using an eyepiece taking some of the light from the detector, and a joystick-controlled motor moving the whole microscope. By removing the filter and thereby using white light it was easy to find the perfect focus as the fringes then were black (zeroth order) instead of brightly coloured. Newer systems are provided with autofocus.

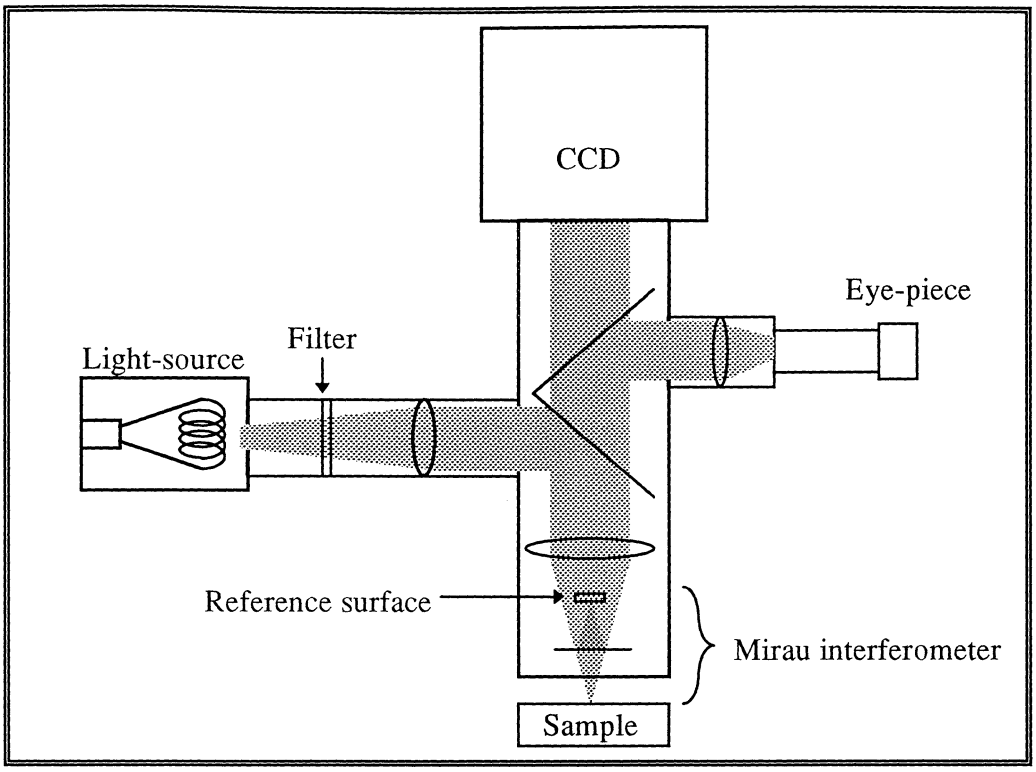

Figure 10. Cross-section of the WYKO.

3.5.1.2.Limits

- The instrument measures over an area of approximately 1x1 mm with the magnification head I used (10x).
- The spatial sampling interval, defined by the detector array was 4 μm.
- The maximum surface heights, defined by the depth of field was 10 μm.
- The maximum slope, defined by the wavelength and the spatial sampling interval was 1,74°.

These three limits made it impossible for me to use the WYKO except for the very smooth samples. The steepness and the height of the surface structures on the other samples made it impossible for the instrument to interpret the fringe pattern. The manual mentioned a measurement repeatability to 0,3 nm *rms*-roughness but this was never of any concern to me since none of the samples had a *rms*-roughness of less than 30 nm.

3.5.1.3.Data

The software supplied with the instrument allows full system control (except focusing), surface calculations, graphic display and statistical analysis. The features mostly used at my experiments were:

- Surface plots - Colour contour
  - 3D
- Power spectrum - Colour contour
  - Profile
- *Rms*-roughness (δ)
- Average roughness (R_a)

3.5.1.4.Summary

The WYKO gave me values on the *rms*-roughness and the R_a for the smoothest samples. The power spectrum of these samples were also studied in order to find any anisotropies of the surfaces. A good impression of the surface structure could be obtained by looking at the sample and the fringes through the eyepiece.

3.5.2. Alpha-Step

Another method for measuring the surface roughness of the samples was using the Alpha-Step 200 from Tencor Instruments. As opposed to the other instruments used, the Alpha-Step is a contact instrument employing a diamond-tipped stylus that scans the surface much like a record-player.

3.5.2.1.Function

The sample is placed on an adjustable table under the stylus. The table is raised by a servo motor until the stylus touches the sample. The stylus is then retracted slightly from the surface. When initiating a scan the stylus is automatically lowered and a pre-set stylus force is applied. The stylus then moves in a line across the surface and it's vertical position is monitored by a Linear Variable Differential Transformer. The output from this is digitised giving a vertical resolution of down to 5 Å. The data is analysed by the instruments CPU and displayed on a video monitor, both graphically as a surface profile and numerically as average height, maximum vertical distance, average roughness etc.

3.5.2.2.Data

Only the R_a (average roughness) was recorded although several other quantities were given.

3.5.2.3.Limits

Vertical resolution: 5 Å defined by the AD-converter.
Horizontal resolution: 400 Å defined by the minimum sampling interval.
Stylus radius: 12,5 µm. This limits the size of the structures I was able to measure (Figure 3).
The most significant limit for this work was the maximum thickness of the samples or in other words the distance between the stylus and the sample table at it's lowest position. As this was only around 20 mm I could only do measurements after having removed the bolt. Naturally this could only be done on samples that would not be used in the electrode and therefore only serve as references.

3.5.2.4.Summary

The Alpha-Step proved to be the most valuable instrument for measuring the surface roughness of my samples. This was due to the fact that it was the only instrument capable of measuring very rough surfaces such as etched or sand-blasted.

3.5.3. Lambda 9

All the samples produced for this work were measured with a Perkin-Elmer Lambda 9 spectrometer. The Lambda 9 is a double beam, double monochromator, UV/Visible/Near Infrared (NIR) spectrometer, in my case used with an integrating sphere to collect the scattered light (Figure 11). It has a total wavelength range of 185-3200 nm using two different light sources, two monochromators and two detectors. I used it to measure total and diffuse reflectance but it works just as well for measurements of transmittance.

3.5.3.1.Function

Light from one of the lamps is spectrally filtered first by one of seven bandpass filters and then by two consecutive turnable gratings. The monochromatic beam is reflected to a chopper assembly that either reflects, blocks or transmits the light. The reflected light hits a focusing mirror and becomes the sample beam. The transmitted light hits another focusing mirror and becomes the reference beam. When the light is blocked the detectors give the "dark" or zero signal.
The sample and reference beams alternately enter the integrating sphere coated with highly reflective, diffuse barium sulphate. The sample beam is scattered by the sample placed over the Sample Port. The reference beam is scattered by a barium sulphate plate placed over the Reference Port. The specular component of the scattered light from the sample hits the Specular Component Aperture (SCA) covered with either a barium sulphate plate (when measuring total reflectance) or a small black plastic cup, called a Specular Component Trap (SCT, when measuring diffuse reflectance).

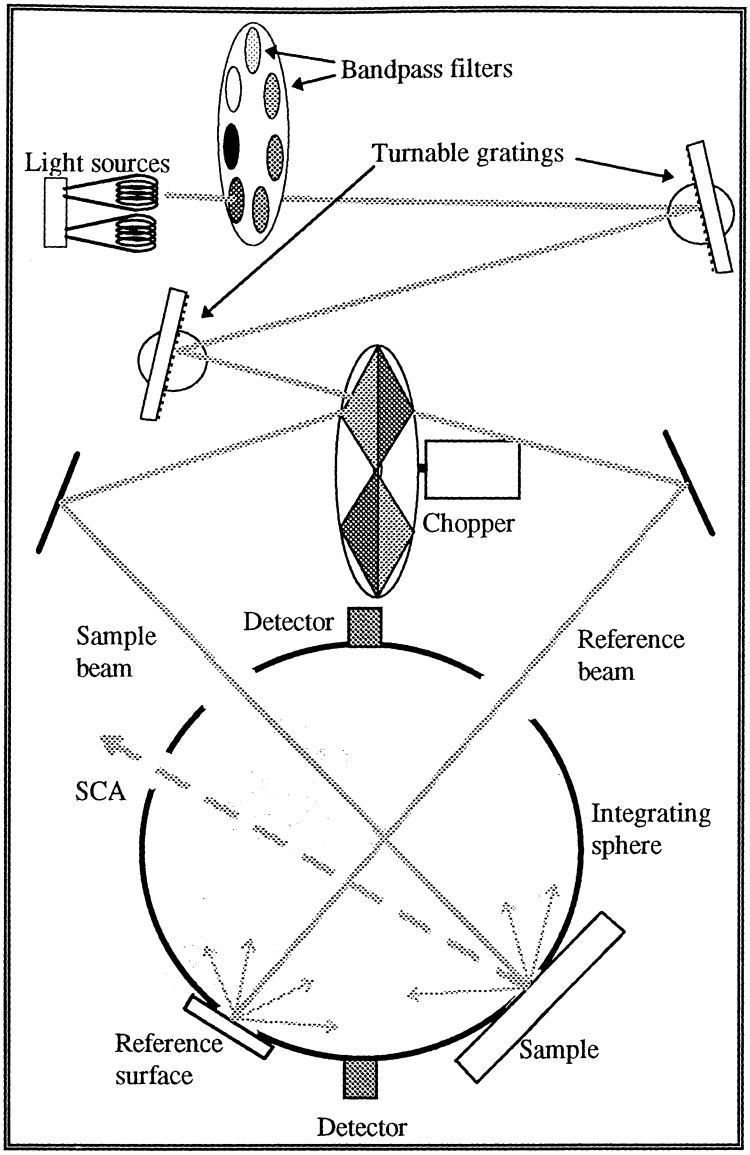

Figure 11. Sketch of the Lambda 9.

Inside the sphere the light instantly reaches a homogenate radiation balance equilibrium due to multiple diffuse reflections on the barium sulphate. A photo multiplier, for UV and Visible, at the bottom of the sphere, and a PbS detector, for NIR, at the top measures this equilibrium radiation. These signals, alternating between sample, reference and dark, are then converted by the spectrograph's microcomputer into a value of reflectance for the sample.

3.5.3.2.Data

The data was automatically sent to a KaleidaGraph file in a Macintosh computer where it was saved as columns of wavelength and reflectance. KaleidaGraph was also used to analyse the data and to plot charts. Later the relevant data was further analysed in Lund.

3.5.3.3.Operation

The lambda 9 needs an hour of warming up to ensure stable measurements. The instrument is then programmed with the desired parameters. A barium sulphate plate is placed in the sample holder and a so called background scan is performed to calibrate the instrument. This is done every time the set-up is changed e.g. when switching from total to diffuse reflectance. The sample is placed in the sample holder and the proper scan is performed. When all samples are measured for total reflectance the white plate covering the SCA is changed for the SCT and the whole procedure is repeated for diffuse reflectance.

3.5.3.4.Summary

The Lambda 9 gave accurate values of the total and diffuse reflectance over a wide spectra. This was used both as a direct characterisation of the samples and to calculate the *rms*-roughness (Ch. 3.4.4) for the smoothest samples.

3.5.4. Angle-Resolved Scattering

Measurements of angle-resolved scattering was done as a complement to the Lambda-9 measurements, to qualitatively study the scattering properties of the surfaces and to maybe be able to calculate the *PSD*-functions of some of the surfaces.

3.5.4.1.Function

The instrument I used for measuring angle-resolved scattering was a scatterometer, constructed and designed in Uppsala, based on a HeNe laser light source and a movable solid-state detector mounted on a turnable arch. The sample was placed in the centre of curvature (along the axis of rotation) of the arch (Figure 12).
The position of the detector was fully controlled by a HP-VEE computer program through two servo motors. The hemisphere above the sample could thus be scanned automatically and the detector signal was registered by the same program. The set-up included a chopper and a lock-in amplifier to improve the signal.
The sample was placed with a small angle of incidence so that the specular component could be measured without blocking the laser beam. Since most of the samples were considered isotropic the scanning was performed only along the plane of incidence, from a few degrees "before" the specular component, all the way down to a grazing angle (along the surface). For a few samples, a scan was also performed perpendicular to this plane

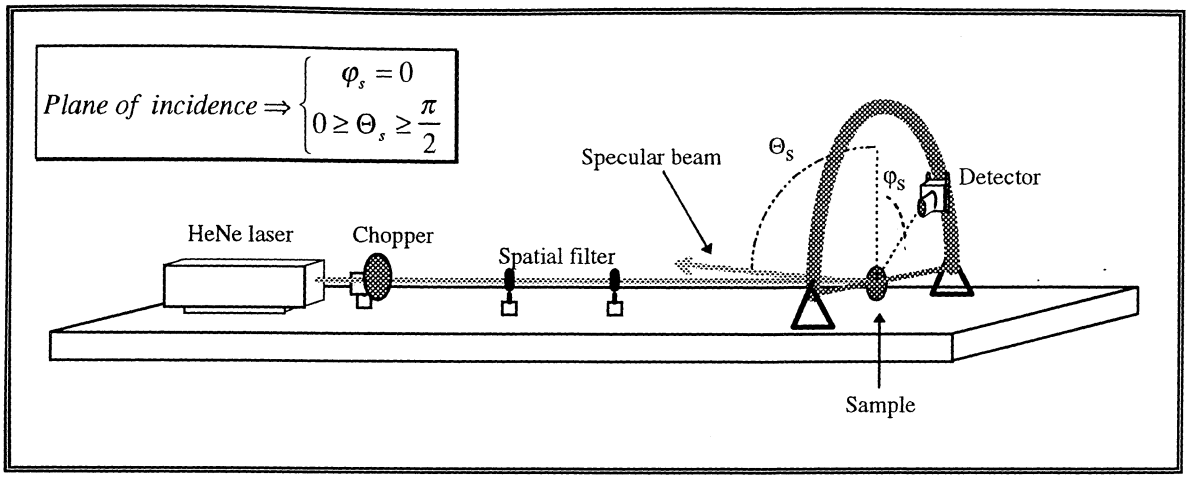

Figure 12. Set-up for angle-resolved scattering measurements.

3.5.4.2.Data

The output from the lock-in amplifier was sent to the PC as uncalibrated values of the average intensity over the area of the detector. These values were saved together with the corresponding angles.

3.6. MEASURING PROCEDURES AND RESULTS

3.6.1. Lambda-9

All samples were measured for total and diffuse reflectance. Scanning was made from 250 nm to 1300 nm (Figures 13 and 14) to see if there would be any radical changes in reflectance for doubled (532 nm) or quadrupled (266 nm) Nd:YAG-light. The bump at 860 nm coincides with the changing of light source. The most interesting thing about these plots is the fact that that the two polished samples (1 and 23) appear very smooth (low diffuse but high total reflectance) for visible wavelength while they become more and more diffuse for shorter wavelength (UV). At 250 nm the specular component (R_{total} - $R_{diffuse}$) is practically zero. This indicates that there are structures in the surface with a spatial wavelength corresponding to UV-light (see Vector Theory, ch. 3.4.5). Sample 24 is obviously even smoother. Although the diffuse scattering starts to rise for shorter wavelengths, the total reflectance remains fairly high testifying that there is still a substantial specular component. This is completely in line with the numerical values of the *rms*-roughness and R_a discovered later.

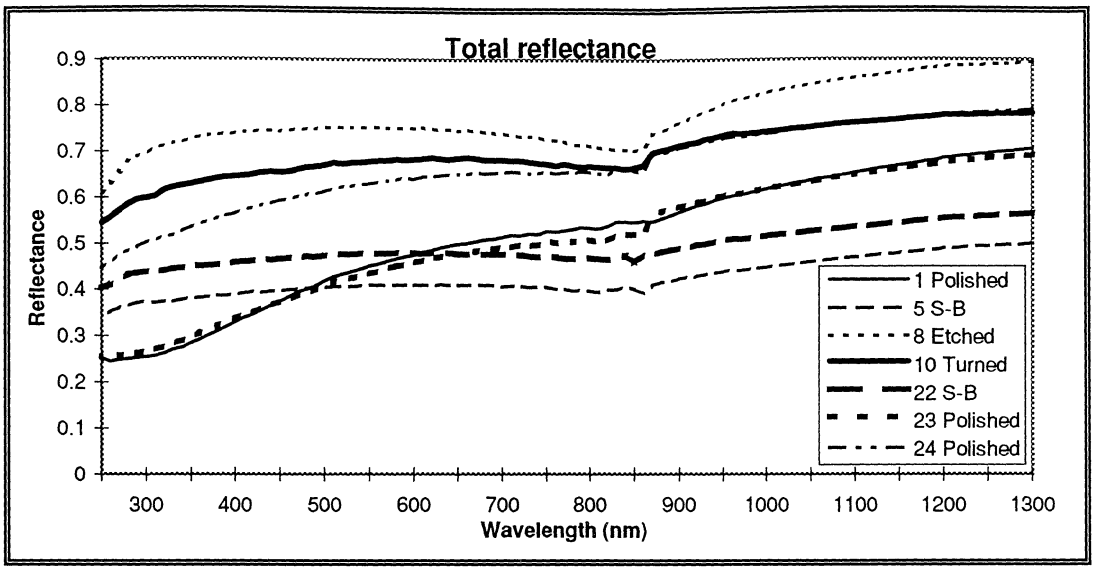

Figure 13. Total reflectance for a selection of samples.

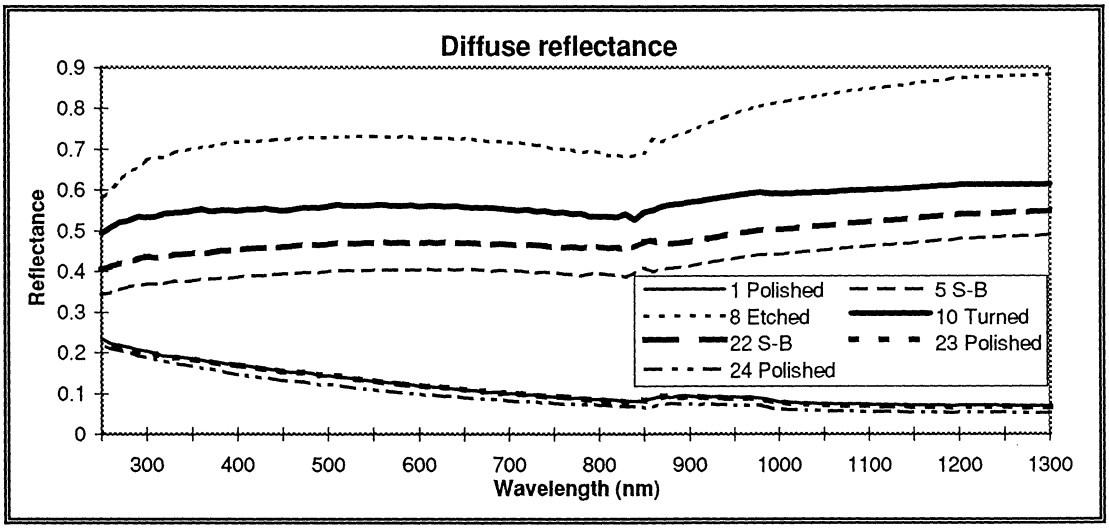

Figure 14. Diffuse reflectance for a selection of samples.

For most of the project though, the important parameter was the total reflectance at the fundamental Nd:YAG wavelength1060 nm (Table 2 and figure 17).
The *rms*-roughness was calculated using the scalar theory. This could however only be done accurately for the polished surfaces (samples 1, 23 and 24) because of the condition for usage of the scalar theory ($\delta << \lambda$). The errors made when using the scalar theory on rougher surfaces can be clearly seen in figure 15 where the *rms*-roughness depends on the wavelength for samples 5, 8, 12 and 22 while it is fairly constant for the polished samples. The *rms* values for the rough samples are also more than a hundred times smaller than according to the Alpha-Step (Table 2).

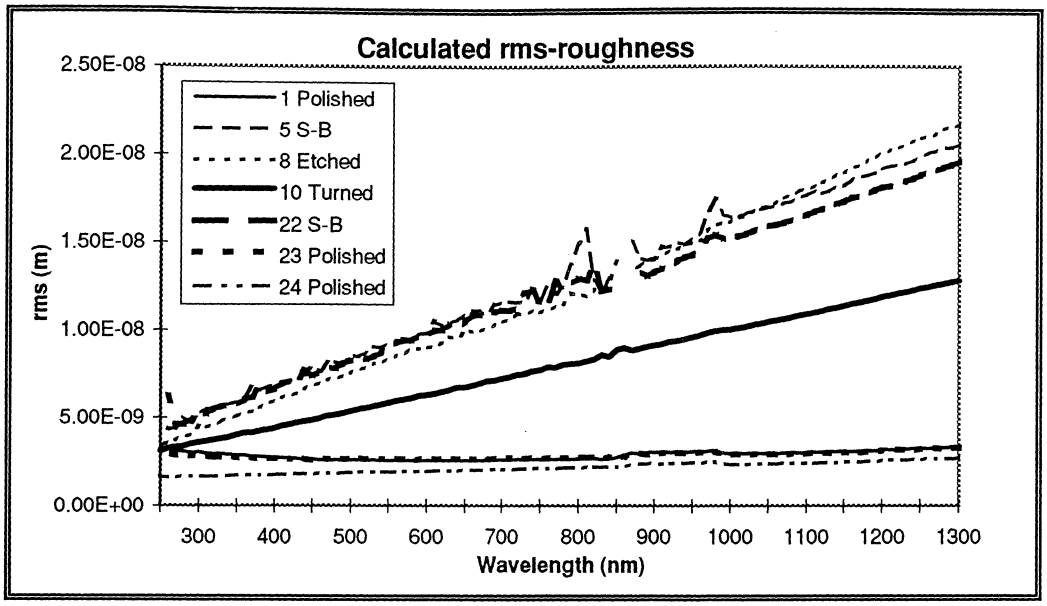

Figure 15. *Rms*-roughness calculated with data from the Lambda 9 spectrometer.

3.6.2. WYKO

The five smoothest samples were measured with the WYKO and the *rms*-roughness and average roughness (R_a) were registered (Table 2). The fact that the *rms* is larger than the R_a indicates that there are a significant number of large deviations from the mean surface level in the form of "bumps" and "holes".

3.6.3. Alpha-Step

All samples with the bolt removed were measured with the Alpha-Step. This method probably gave the best values of the *rms*-roughness (Table 2). It limits the *rms*-roughness downwards. With a stylus as big as 12,5 μm it is quite likely though, that the real values are substantially higher. The Alpha-Step gives nevertheless a good relative scale with which to compare the samples.

3.6.4. Angle-Resolved Scatterometer

All samples on which the bolt had been removed where run in the angle-resolved scatterometer. The data was calibrated by integrating over all angles (hemisphere) and comparing the sum to the total reflectance at 630 nm as determined with the Lambda 9 (Eq. 9).

$$R_{tot} = \int_0^{\pi/2} \int_0^{2\pi} BRDF \cdot \cos\Theta \cdot \sin\Theta \cdot d\Theta \, d\varphi \tag{9}$$

This made it possible to calculate the *BRDF* (Figure 16).

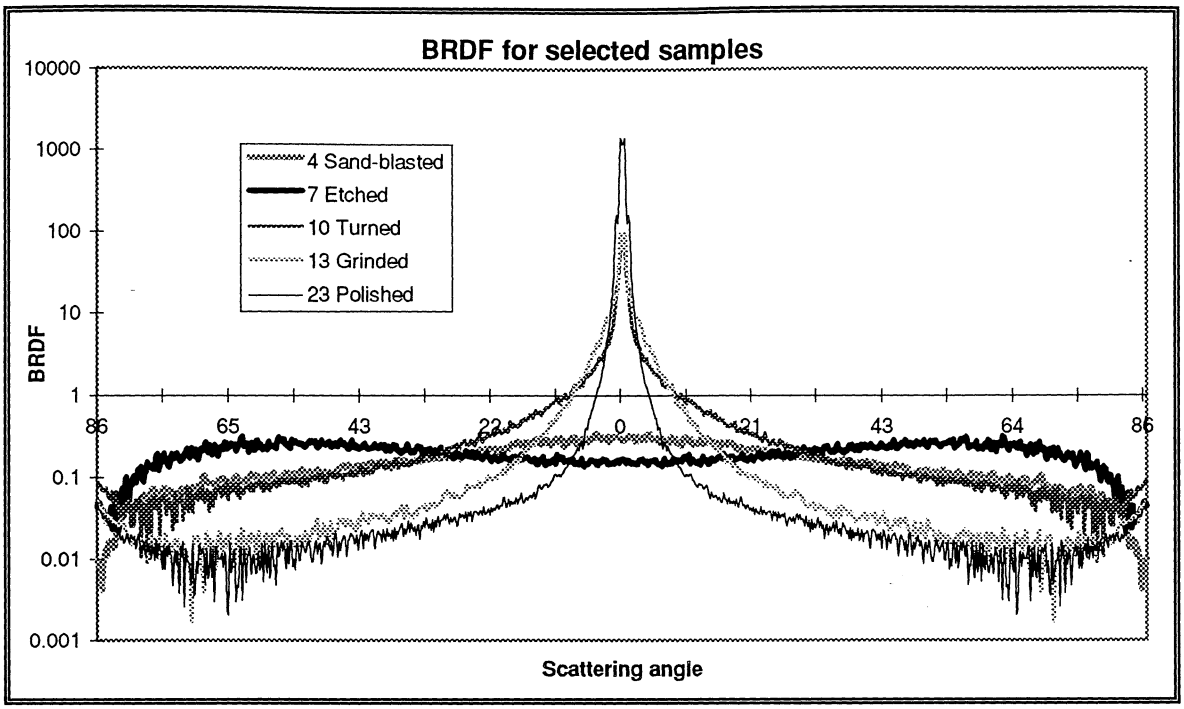

Figure 16. *BRDF* as a function of the scattering angle.

The determination of the *PSD* and the surface profile is fairly complicated and was not performed. Some comments can however be made about the results.

- The etched surface has an almost constant *BRDF* (Lambertian surface).
- Sample seven and twenty-three, although with similar reflectance have completely different scattering properties. Of course, this conclusion can be made by just looking at the two surfaces.
- There is a qualitative difference in scattering between the etched and the sand-blasted samples.
- The fairly high reflectance of the raw (turned) surface can be explained by the combination of a strong specular component and considerable diffuse scattering.

3.7. CONCLUSION OF SURFACE CHARACTERISATION

It is possible to dramatically change the absorptance of an aluminium surface by simple processing. With a couple of seconds of sand-blasting the absorptance at 1060 nm was increased from 23% to 54%. It is not however certain that making the surface rough will increase the absorptance. Etching with sodium-hydroxide and thereby substantially increasing the roughness of the surface actually decreased the absorptance to less than 20% while polishing in some cases increased it to more than 40% (Table 2).
For the triggering experiments the *rms*-roughness and the absorptance at 1060 nm must therefore be considered as two separate parameters.

Surface characterisation			Calculated rms/R_A (nm)			
	Sample	R_{tot}-1060	Lambda-9	rms-WYKO	R_A-WYKO	R_A-Alpha-Step
Polished	1	0.641	30	72	55	
	23	0.637	28	73	54	91
	24	0.752	23	33	26	
Grinded	13	0.537		45	33	65
	2	0.566		83	62	
	12	0.770				323
	14	0.774				
Raw	10	0.755				1347
(turned)	3	0.770				
Sand-blasted	5	0.462				
	4	0.499				1712
	21	0.503				2626
	22	0.529				
	17	0.608				
	18	0.612				2386
	19	0.616				
	20	0.623				6327
	16	0.672				1801
	15	0.673				
Etched	9	0.772				
	11	0.774				
	7	0.783				3531
	6	0.815				1224
	8	0.849				

Table 2. Results of surface characterisation.

From these data it can also be seen that the randomness in the surface processing is fairly small. The two samples in each pair have very similar characteristics regarding the reflectance at 1060 nm (Figure 17).

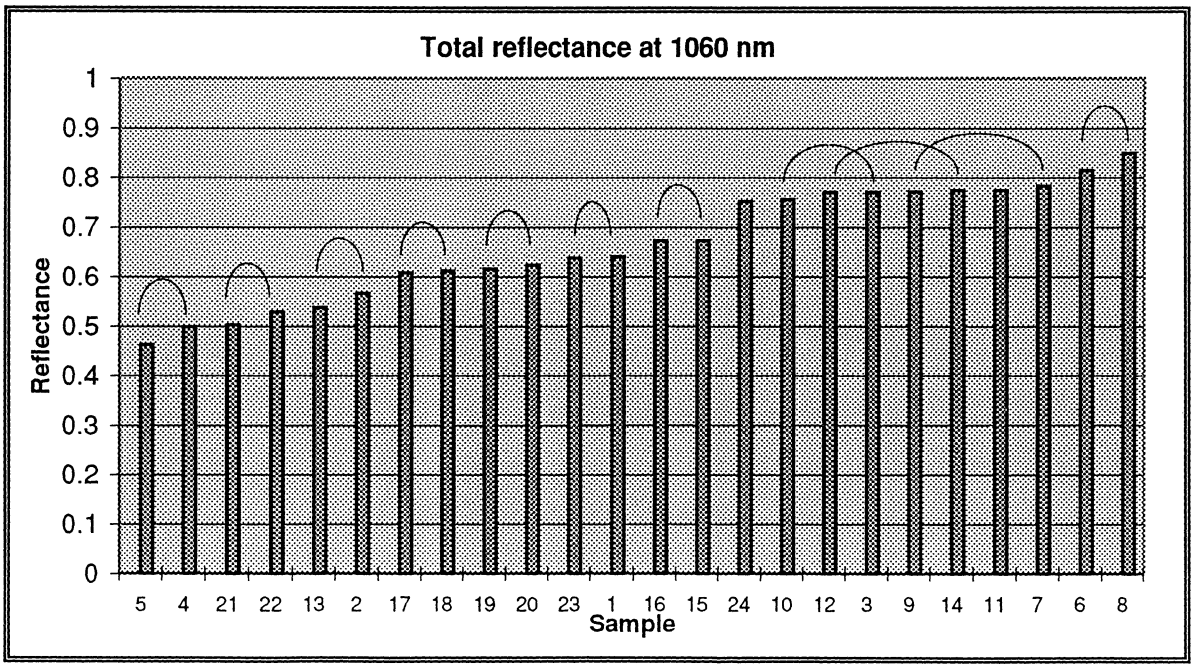

Figure 17. R_{tot} at 1060 nm in corresponding pairs.

Regarding the methods of surface characterisation I make the following conclusions:

- Optical (non-contact) methods of determining the surface roughness are not appropriate for the rough surfaces used in this project. They are developed for optical and other very smooth surfaces and are limited mainly by the wavelengths used.
- No explicit relationship between the surface roughness and the absorptance was observed in the measurements.

4. Laser Triggered Spark Gaps

This section deals with the part of the project performed in Lund. It starts with an introduction to laser triggering. Chapter 4.2 describes some of the statistical methods used in high-voltage engineering and chapter 4.3 describes the experimental set-up and also includes the special safety arrangements. Chapter 4.4 deals with the actual measuring procedures for the different experiments performed and chapter 4.5 summarises all the results.

4.1. THEORY

4.1.1. Electrical Breakdowns

An electrical breakdown occurs if the field is sufficiently strong to produce more free electrons than are absorbed in the gas. Free electrons are being produced through collisions with the gas molecules. This ionisation can take place without any external electric field but at room temperature the kinetic energy of the electrons is too small to knock out more new electrons than are being lost through recombination and attachment (Eq. 10).

(10) $$X^+ + e^- \xrightarrow[recombination]{} X \qquad X + e^- \xrightarrow[attachment]{} X^-$$

With a sufficient field the electrons are accelerated between each collision and gather enough kinetic energy to ionise several molecules. A chain reaction has thus started, increasing the amount of free electrons exponentially until the gap breaks down (Figure 18).

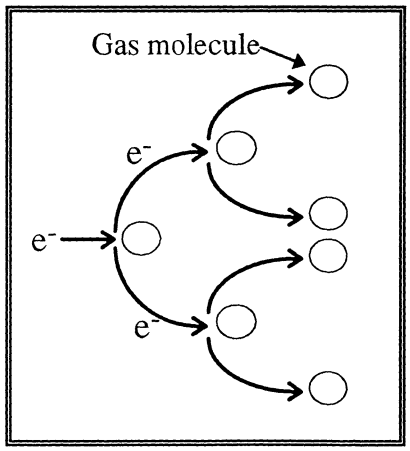

Figure 18. Avalanche of ionisation.

4.1.2. Laser Triggering

In most literature, a clear distinction is made between volume triggering and surface triggering (Figure 19). In volume triggering the laser pulse interacts with the gas only. The laser beam can then be directed either perpendicular or parallel to the electric field in the gap. In surface triggering the laser pulse also interacts with the surface of one of the electrodes. In this case the beam is most often directed parallel to the field.

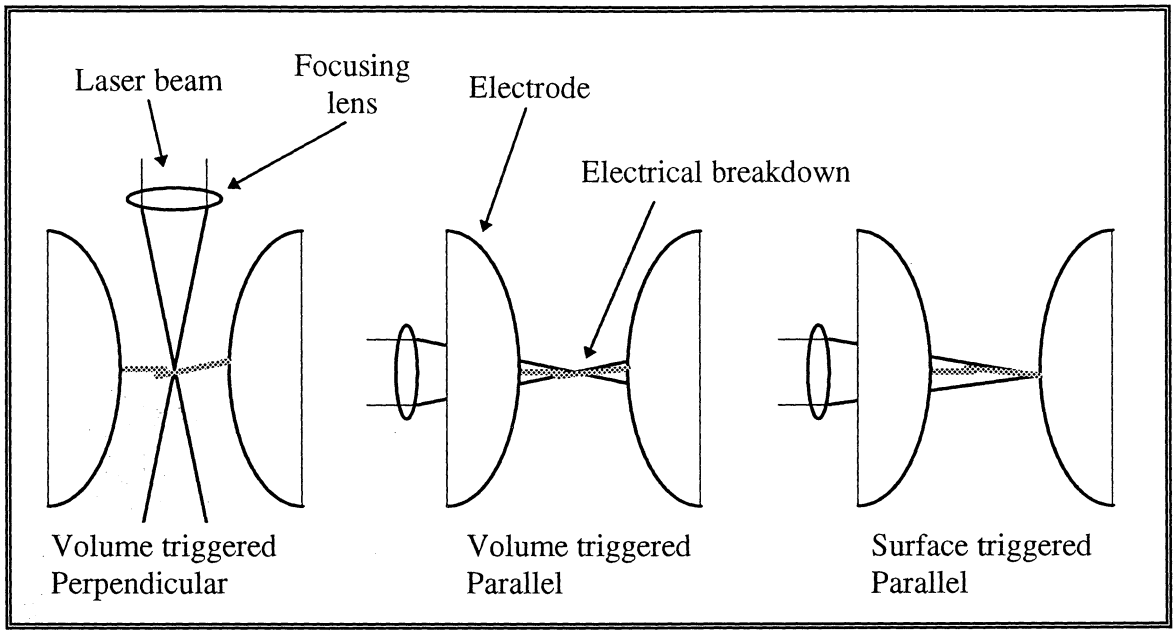

Figure 19. Three types of laser triggered spark gaps.

The laser pulse tears the molecules, either in the gas (volume triggering) or on the electrode surface (surface triggering) apart, creating a highly ionised plasma (optical breakdown). This is done by multi-photon absorption and inverse bremsstrahlung. Inverse bremsstrahlung is when free electrons are accelerated by the laser field in such a way that they hit surrounding molecules with enough kinetic energy to ionise them. In most cases the plasma is ignited by multi-photon absorption. Once there are some free electrons, inverse bremsstrahlung will be the dominant process, especially when using low frequency (IR) lasers as in my case. The plasma is opaque to the light why most of the pulse actually interacts with the plasma surface causing it to grow rapidly.
Surface charges on this conducting bubble will shield it's inside from the applied electric field and thereby enhance the field just outside the plasma. This locally enhanced electric field causes further ionisation along the direction of the field. The plasma will thus extend in that direction (Figure 21). Surface charges will be drawn to that spot and increase the local field even more and so on. This extension of the plasma in the form of a channel along the direction of the field is called a streamer. These streamers can be of both polarities and take different shapes [6] but this will not be further discussed here. The streamer propagates across the gap and eventually closes the gap causing a complete electrical breakdown (Figure 20).

Since it is the absorption of laser energy at the surface of the electrode that creates the plasma that triggers the breakdown, it was assumed that by increasing the roughness of the sample and thereby augmenting the absorptance it would be possible to lower the pulse energy needed to get a triggered breakdown at a specific gap voltage.

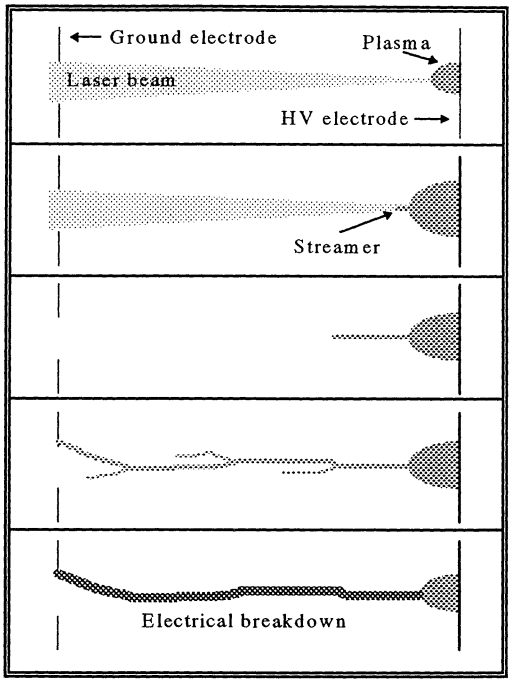

Figure 20. Streamer propagation.

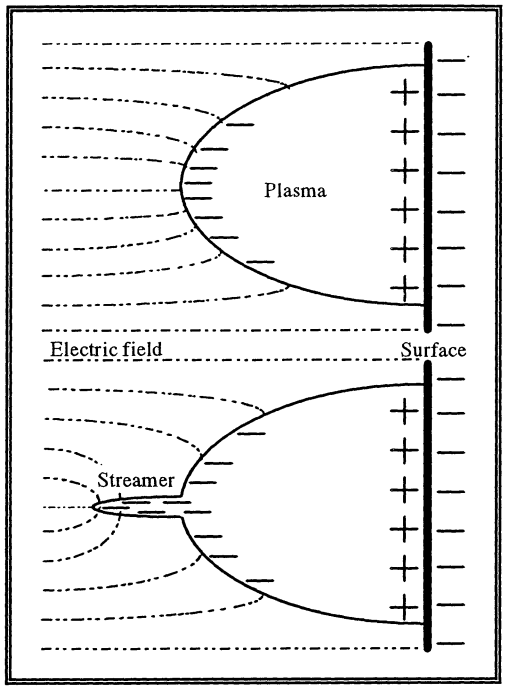

Figure 21. Close-up of streamer formation.

4.2. STATISTICS

In high-voltage engineering and especially when analysing breakdown processes it is common to use the Weibull distribution [7]. The Weibull distribution is an extreme-value distribution limited in one direction (downwards) with the three parameters:

x_0 : initial value (downward limit)
δ: Weibull exponent (measure of dispersion)
$h = x_{63} - x_0$ (63% quantile)

In my calculations x_0 was however set to zero thus reducing the amount of parameters to two.

The density function of the Weibull distribution is:

$$f(x) = \begin{cases} \frac{\delta}{\eta}\left(\frac{x-x_0}{\eta}\right)^{\delta-1} \exp\left[-\left(\frac{x-x_0}{\eta}\right)^{\delta}\right] & x > x \\ 0 & x \le x_0 \end{cases} \tag{11}$$

This gives a distribution function as follows (Eq. 12, figure 22):

$$F(x) = \begin{cases} 1 - \exp\left[-\left(\frac{x - x_0}{\eta} \right)^{\delta} \right] & x > x_0 \\ 0 & x \le x_0 \end{cases} \tag{12}$$

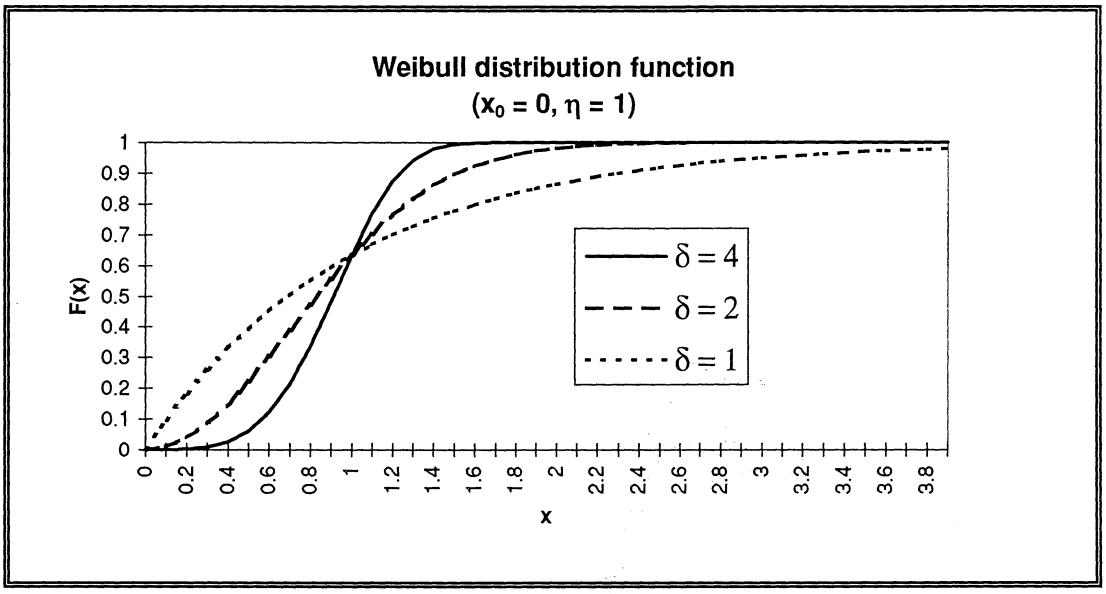

Figure 22. Weibull distribution function.

By a simple transformation (Eq. 13, 14 and 15) the Weibull distribution can be represented as a straight line. Plotting the data on so called Weibull probability paper (Figure 27), designed through this transformation, makes it easy to conclude if the data correspond to the Weibull distribution and to calculate the Weibull exponent (δ). As seen below (Eq. 15) the exponent comes out as the slope of the line. The Weibull exponent is an important parameter of the stability of the system as it determines what voltage interval that corresponds to a rise in breakdown probability from for example 0.01 to 0.99.

$$F(x) = 1 - e^{-\left(\frac{x}{\eta}\right)^{\delta}} \tag{13}$$

$$\ln\left(\frac{1}{1 - F(x)} \right) = \left(\frac{x}{\eta} \right)^{\delta} \tag{14}$$

$$\ln\left(\ln\left(\frac{1}{1 - F(x)} \right) \right) = \delta \cdot \ln(x) - \delta \cdot \ln(\eta) = \quad k \cdot \ln(x) + C \tag{15}$$

4.3. EXPERIMENTAL SET-UP

The breakdown experiments were performed in the HV-lab at the Department of Physics at Lund Institute of Technology. The experimental set-up consisted of two separated tables, one with the laser equipment and one with the high-voltage (HV) equipment. This second table was surrounded by an grounding metal cage for safety reasons.

4.3.1. Optical Set-up (Figure 23)

4.3.1.1.Laser

The laser used was a Quanta Ray DCR-1 Nd:YAG laser from 1979, emitting at 1064 nm. It consists of a refrigerator-sized power supply module, a 140x30x40 cm laser module and a remote control connected by chord.
The pulse width was approximately 8 ns and the pulse repetition rate was set to the minimal 2 pps to simplify single shot performed using the Q-switch-button on the remote control.
To minimise changes in the pulse mode due to changes in the thermal focusing in the laser cavity, the flash-lamp (pumping) power was kept constant throughout the experiments. Instead the laser power was controlled by a polariser outside the cavity. I used pulse energies between 2 and 80 mJ.
A harmonic generator placed after the amplifier enabled frequency doubling, tripling and quadrupling although this was never used for the project.
The first component outside the laser was an optical isolator, protecting the laser from back scattering. After that a IR-reflecting mirror was placed to deviate the beam towards the HV-table.

4.3.1.2.HV-table

The beam enters the cage and reaches a mirror reflecting 50% of the power towards the electrodes. The rest is transmitted to a calorimeter used to monitor the pulse energy. The reflected beam reaches a plane-convex lens. The pulse is thus focused through a hole in the ground electrode into the electrode gap. The focusing lens could be moved to alter the position of the focus. The focal length of the lens was chosen to 25 cm to ensure a clear passage through the hole. Due to the distance from the laser and the divergence of the beam, it was not necessary to expand the beam before focusing it. Before the lens the beam diameter was approximately 14 mm giving a theoretical minimum beam diameter of 50 μm at the focus.

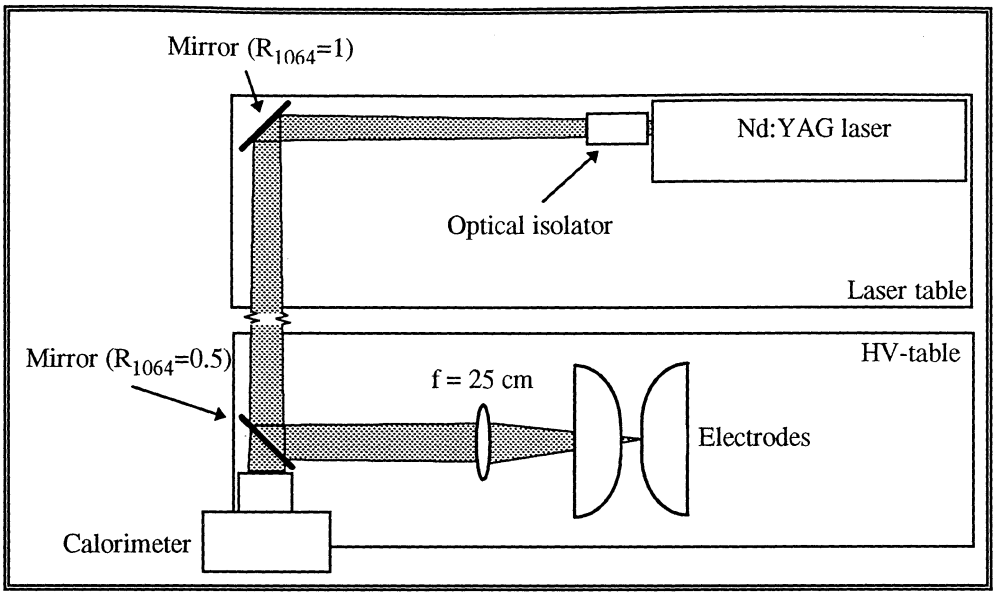

Figure 23. Optical set-up.

4.3.2. High-Voltage Set-up (Figures 24 and 25)

Under the HV-table a high-voltage power supply (FUG) was placed together with an automatic fuse (FUG-killer) turning off the power supply at high currents (breakdown). On the front-panel of the power supply the polarity and the voltage could be controlled. The voltage could be set in the range of 0 - 63 kV with an accuracy of 100 V. The power supply also monitored the current to the electrode indicating the leakage from glow discharges to the air and currents through the supporting structure of the HV-electrode down to the table (ground). A lot of effort was put into minimising this current by insulating the electrode with tape.

The high-voltage was passed to the HV-electrode through a well insulated cable and a 150 MΩ resistor. The electrode was also connected to a 2000 pF (400 kV) capacitor and a capacitive voltage divider used to monitor the breakdown. The capacitor was used to get sufficient amount charging to ensure a complete breakdown despite the shutting down of the power supply. The capacitor provides stable gap-voltage throughout the pre-breakdown phase despite the leaking currents and other loss of energy caused by the streamer formation and propagation.

The ground electrode, the bottom of the capacitor, the voltage divider and the protective cage were all connected to a long copper sheet on the table grounded through the power supply.

4.3.2.1.Electrodes

The electrodes were held in place by a structure of insulating synthetic plywood (Appendix A, figure 40). The axis of symmetry of the electrodes was parallel to the optical axis of the laser beam. A small off-axis displacement was made so that after turning the sample slightly the laser pulse would hit new, undamaged surface.
The electrode gap was chosen to 20 mm to ensure spontaneous breakdown at a voltage below the maximum voltage of the power supply.

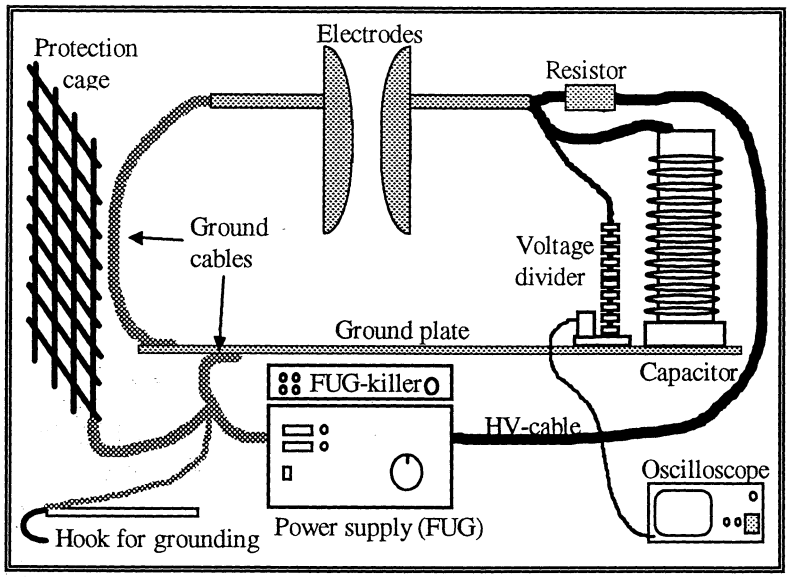

Figure 24. HV components.

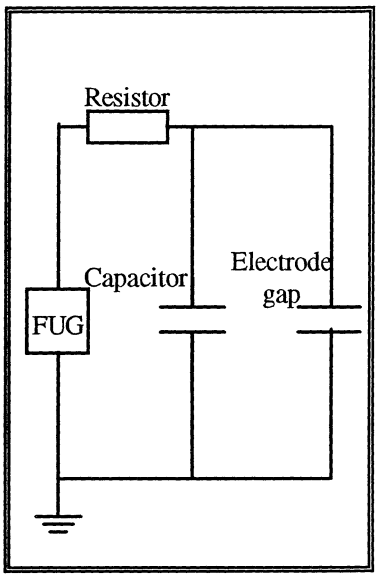

Figure 25. HV components.

4.3.3. Monitoring

As mentioned before the pulse energy for each shot was measured with a calorimeter.
The gap voltage was given directly by the power supply although it had to be corrected by subtracting the voltage over the resistor equalling the leakage current multiplied with the resistance (150 MΩ).
The delay time between the laser pulse and the breakdown was measured using an optical fibre, a photo diode, and an oscilloscope (Figure 26). The optical fibre collected light from the laser-induced plasma and from the breakdown arc and the time difference gave the delay time.
That the second light pulse actually corresponded to the breakdown was confirmed by connecting the voltage divider to the same oscilloscope. Unfortunately I was never able to calibrate this voltage probe.

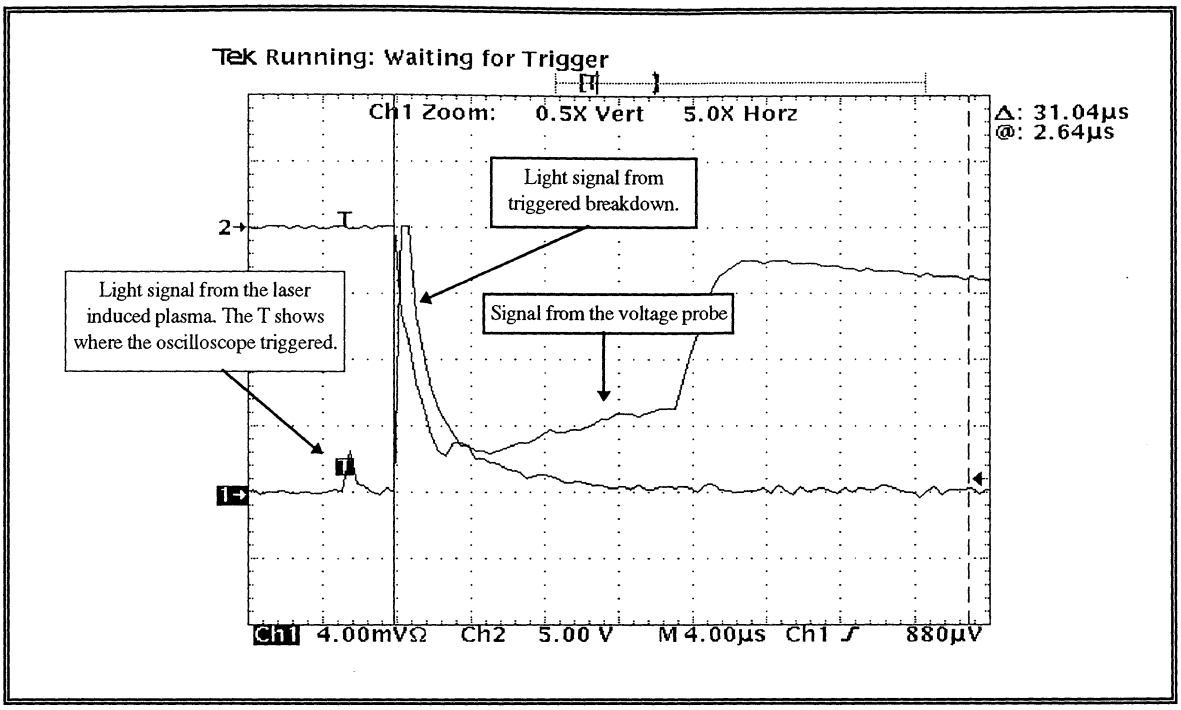

Figure 26. Oscilloscope showing triggered breakdown.

After all the triggering experiments had been performed, I rigged a CCD-camera beside the electrodes and was thereby able to take digital "snap-shots" of the breakdown processes. The camera was triggered by a Q-switch-synchronised output on the laser. The pictures were saved in a PC and could later be edited using Adobe PhotoShop.

4.3.4. Safety

The two major safety problems in this project were naturally the laser and the high-voltage. The fact that light with a wavelength of 1064 nm is invisible made it extra dangerous to the eyes since the pupils remain big despite strong radiation. It also made it hard to keep track of the beam through the system. Light sensitive paper and an IR-viewer were used to localise the beam and safety-goggles were used at all times to protect the eyes. Curtains covered the windows to prevent the beam or reflections to escape outside the room and a warning light was lit outside the door of the lab.
60 kV and a large capacitor guaranteed a lethal environment around the HV-table and called for extra precautions when performing the experiments. As mentioned before a grounded metal cage was placed around the HV-table. Before entering the cage to adjust the sample or the set-up, all HV-components (electrode, capacitor, HV-cable etc.) had to be grounded with a large copper hook connected to the ground cable of the power supply.

4.4. MEASURING PROCEDURES

The first step after lining up the optical system is to measure reflectance of the second mirror to calibrate the calorimeter. It was discovered that the mirror reflected 50% of the incoming radiation.

A few measurements of spontaneous breakdown were made to test the set-up. Leaking current proved still too high (>60 μA) why the insulation of the HV-electrode had to be improved with tape and a wooden board between the supporting structure and the table. The leaking current was reduced to less than 20 μA at 60 kV.

Measurements were now made on one very smooth sample (sample 1) and one fairly rough (sample 5). The results from these measurements were later omitted since the laser energy had been adjusted by changing the flash lamp power. This alters the thermal-focusing in the cavity and thereby the focus at the electrode. From then on the flash lamps were kept constant at full power (100 J/pulse) on the oscillator and approximately half power (50 J/pulse) on the amplifier. Observe that these values are the lamp inputs and not the laser output. The adjustment of laser energy was then made with a movable polariser in combination with the polariser in the optical isolator.

The focusing lens could be moved along the optical axis, thereby moving the focus. The polarity of the HV-electrode could also be switched.

4.4.1. Spontaneous Breakdown

For determining the voltage required for spontaneous breakdown, the laser is turned off. A right sample is put in place by carefully tilting the supporting structure of the HV-electrode. The electrode gap is adjusted to the proper length (20 mm) by using a 20 mm wide metal ruler. The HV power supply is turned on and set to a voltage where the probability of spontaneous breakdown is minimal (40 kV). The voltage is then slowly increased while monitoring the current and then voltage displays on the power supply. When spontaneous breakdown occurred, the FUG-killer automatically shut the power supply off and the last current and voltage readings were noted. This procedure is then repeated fifteen times to get a statistically good set of data to make a Weibull diagram.

4.4.2. Triggered Breakdown

For measuring laser triggered breakdown, the oscilloscope is set to appropriate trigger level and scales. The laser is turned on but the Q-switch is kept closed. The laser energy is adjusted with the polariser to a fairly low level (<10 mJ/pulse) while keeping the sample covered. The sample and the electrode is adjusted so that the laser pulse will hit an undamaged part of the surface. The HV power supply is switched on and set to a voltage well below the assumed limit for triggered breakdown. The calorimeter is reset. A laser pulse is fired and one of the following events happens.

- A breakdown occurs. The gap voltage is obviously to high. The whole procedure is repeated at a lower voltage.
- No breakdown occurs but the pulse energy is more than 10% off the average value at the set level. The calorimeter is reset and a new pulse is fired.
- No breakdown occurs and the pulse energy is considered okay. The voltage is then increased by 200 V. The calorimeter is reset and a new pulse is fired. This is repeated until breakdown occurred. Then pulse energy, delay time, voltage and leaking current are noted. The sample is turned slightly so that the next pulse will hit a clean spot and the whole procedure is repeated until fifteen sets of data have been recorded.

The pulse energy is then changed and a new set of measurements is made. This is repeated for four to six different pulse energies.

4.4.3. Measurements

Samples 5, 8, 19, 22 and 24 were picked out as they represented a wide range of surface processing methods, roughness values and absorptance values (Table 3).

Surface characterisation						
			Calculated rms/RA (nm)			RA-Alpha-Step
	Sample	Rtot-1060	Lambda-9	rms-WYKO	RA-WYKO	of corresponding
						sample
Polished	24	0.752	23	33	26	
Sand-blasted	5	0.462				1712 (sample 4)
	22	0.529				2626 (sample 21)
	19	0.616				6327 (sample 20)
Etched	8	0.849				1224 (sample 6)

Table 3. Characteristics of samples selected for triggering experiments.

Measurements of spontaneous and triggered breakdown were made for all these samples with the laser focused just outside the sample-surface and the polarity of the HV-electrode positive.
Samples 22 and 24 were then selected for the remaining experiments. The focus was moved to several places along the optical axis. Measurements were made on the two samples with different pulse energies and with both polarities on the HV-electrode. The most extensive testing was made on sample 22. It was selected since it had been easy to process (sand-

blasting) and since a laser shot at the polished sample (24) changed the surface structure more thus altering the circumstances for each shot.
The plasma limit or the minimum pulse energy required to produce a visible plasma was determined for a polished (24), an etched (8) and a sand-blasted (5) sample. These energies were however so low that it became difficult to get reliable readings from the calorimeter. Pictures of plasmas and breakdown arches were taken with various samples, pulse energies and voltages.

4.4.4. Processing of Data

The relevant parameters for comparing the breakdown characteristics of the different samples are:

- The pulse energy needed to generate a triggered breakdown for a specific gap voltage.
- The delay time for each breakdown (time between triggering and breakdown).
- The jitter or the difference in delay time from one shot to another.
- The U_{50} or the voltage that gives a probability of 0.5 for triggered breakdown.
- The Weibull exponent, δ (not to be mixed up with the *rms*-roughness).

A standard spreadsheet was made to allow the calculations of these and the plotting of a Weibull-diagrams for each series of data.

4.5. RESULTS

4.5.1. Focus on the Surface

The main object of this project was to compare the breakdown characteristics of different surfaces.
The diagram below (Figure 27) shows the cumulative breakdown probabilities of sample 19 for different pulse energies plotted on Weibull distribution probability paper. The diagrams for the other samples are very similar. It is evident that with increasing pulse energy the gap voltage required for triggered electrical breakdown is reduced. The reason for this becomes rather obvious when studying pictures of the plasma at different pulse energies and remembering that the plasma is a highly ionised, highly conducting fireball (Figure 28).

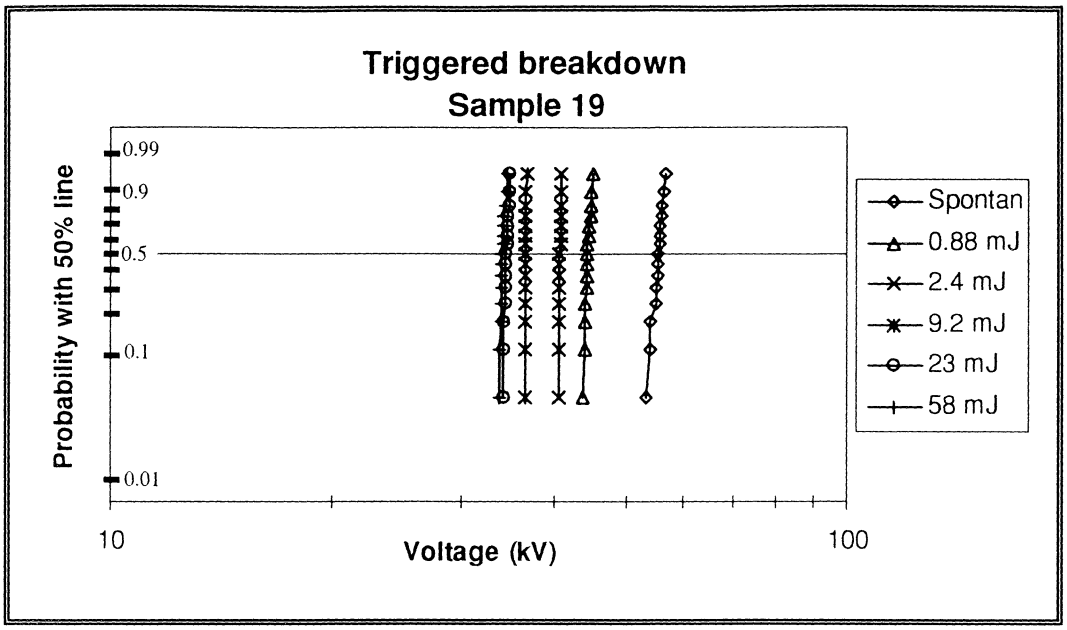

Figure 27. Weibull diagram of triggered breakdown on sample 19.

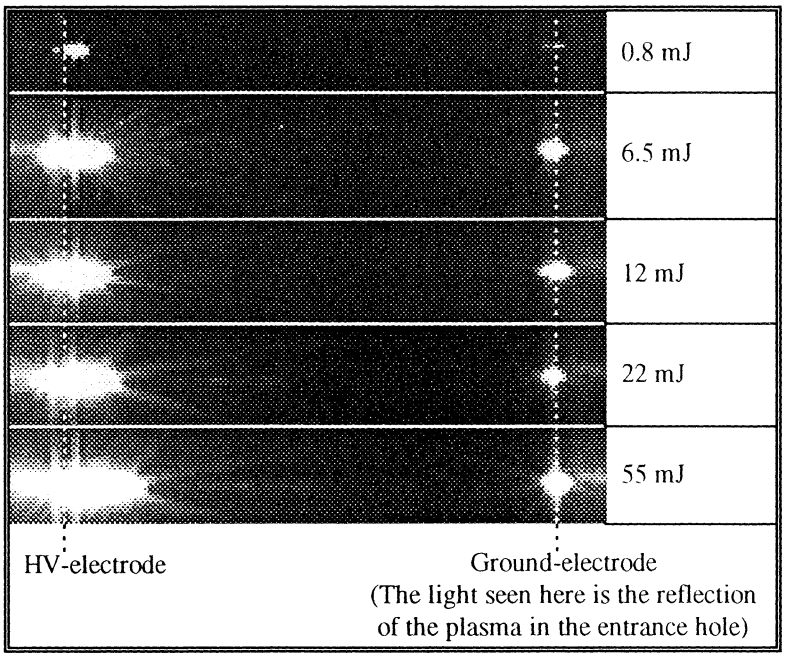

Figure 28. Plasmas at various pulse energies.
(Note that the aperture of the CCD-camera is two steps smaller in the last two pictures, thereby reducing the size of these plasmas to some extent.)

It seems however as if there is a lower limit in voltage gap. This becomes more clear in a diagram showing the U_{50} plotted against the pulse energy. In figure 29 this has been done for all five surfaces.

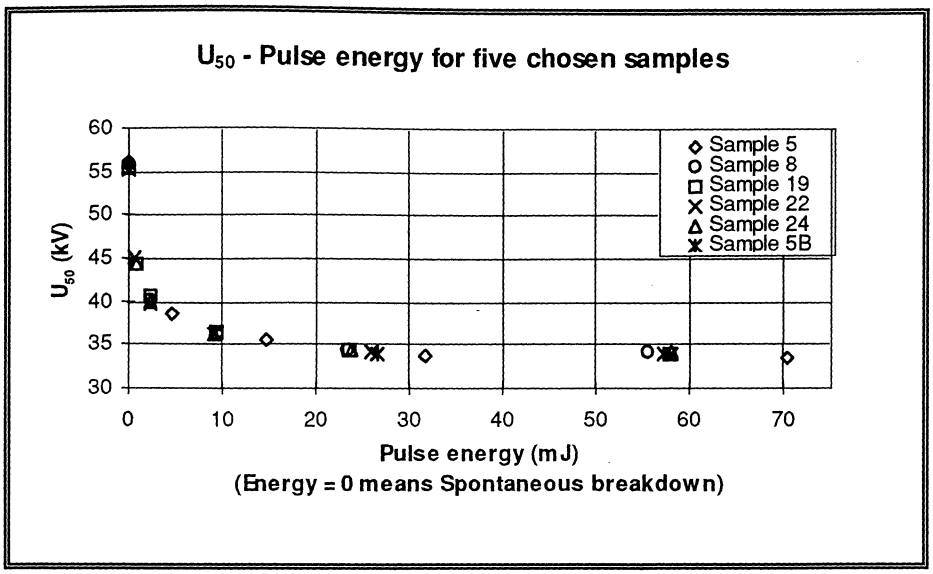

Figure 29. U_{50} versus pulse energy for five samples.

Here we find the first real surprise and probably the most important discovery of my project. All five surfaces give almost identical results. Sample 5 shows a small deviation from the rest at high pulse energies but two additional tests (5B) decreased the spreading of the data further. The deviation is in any case not significant considering the errors involved. The errors here are estimated to +- 0.1 kV on the ordinate and +- 1 mJ on the abscissa. Error bars are excluded to avoid making the diagram unclear.

It can also be seen that the spontaneous breakdown voltages are practically the same for all samples indicating that if a difference in the triggered breakdown voltages had been found, this difference would not have been because of the electrical properties of the surface but rather because of the optical.

Finally, no differences in plasma size or shape can be seen when analysing pictures of laser interaction with different surfaces at pulse energies ranging from one to fifty mJ. However the plasma limit or the lowest pulse energy required to produce a plasma seemed slightly lower for sample 5 with high absorptance than for samples 8 and 24 with low absorptance (Table 4).

Sample	Absorptance	Plasma limit
5	0.54	0.05 mJ
8	0.15	0.06 mJ
24	0.25	0.06 mJ

Table 4. Plasma limit.

Although the measurements were inaccurate due to the problems with the calorimeter at low energies, there is no doubt about the fact that there was a difference in plasma limit between the three samples.

The next parameter to study is the delay time. Table 6 (Appendix B) include all the measured delay times from the five samples. It can be seen that the jitter (dispersion) is devastating except for very high voltages (low pulse energies).

There is also a trend of decreasing delay time with increasing voltage although there are a few exceptions. A little bit surprising considering the results above is that there seem to be a difference in delay times for the different samples. There is no correspondence between the difference in delay time and the roughness or the absorptance of the samples though. The almost astronomical standard deviations (jitter) for lower voltages also make the differences insignificant.

For high voltages where the standard deviation is small, no differences between the samples can be seen. In this part of the diagram (U > 40 kV) there actually seem to be a more simple relationship between the voltage and the pulse energy (Figure 30).

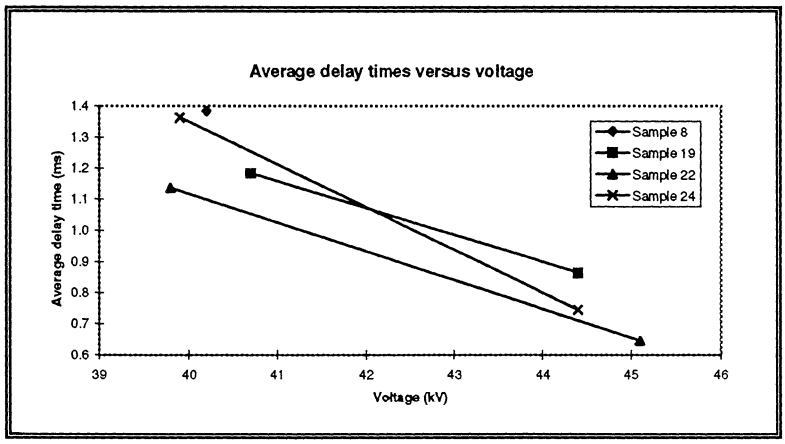

Figure 30. Average delay time versus voltage for U > 40 kV.

The final parameter to investigate is the slope of the line fitted to the cumulative breakdown probability when plotted on a Weibull probability paper. Below is a table and a diagram with these slopes corresponding to different samples and different voltages (Table 5 and figure 31).

	Slope of Weibull diagram (δ)									
	Sample 5		Sample 8		Sample 19		Sample 22		Sample 24	
	U_{50}	Slope	U_{50}	Slope	U_{50}	Slope	U_{50}	Slope	U_{50}	Slope
Triggered	33.4	181	34.1	129	34	137	33.8	184	34.2	209
	33.8	135	34.3	208	34.4	160	34.1	207	34.4	150
	33.8	200	36.3	193	36.4	325	36.3	400	36.2	292
	34	200	40.2	324	40.7	390	39.8	843	39.9	505
	35.5	263			44.4	142	45.1	227	44.4	108
	38.5	318								
Spontaneous	56.1	87	55.8	77	55.3	70	55.2	92	56	112

Table 5. Weibull exponent versus U_{50}.

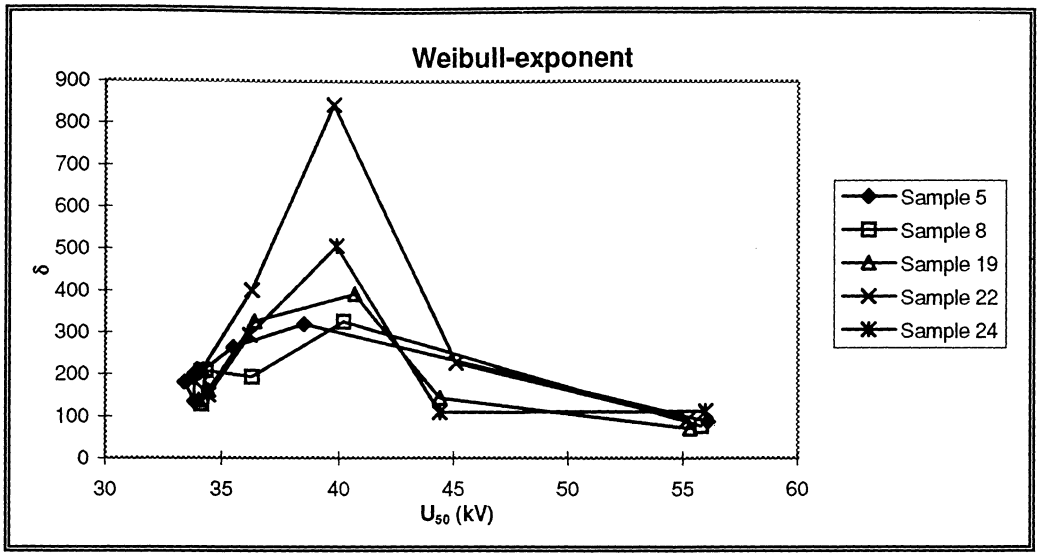

Figure 31. Weibull-exponent versus U_{50}.

It can be seen that spontaneous breakdown gives a larger dispersal (lesser slope) although one must be careful comparing these as the measurements are not done in identical manner (4.4.1 - 4.4.2). Altogether it is difficult to analyse this data quantitatively considering the discrete voltage levels in the triggered measurements..
Another way of comparing the quality of the triggering mechanism is to plot the Weibull diagram with two-sided confidence limits (Figure 32).

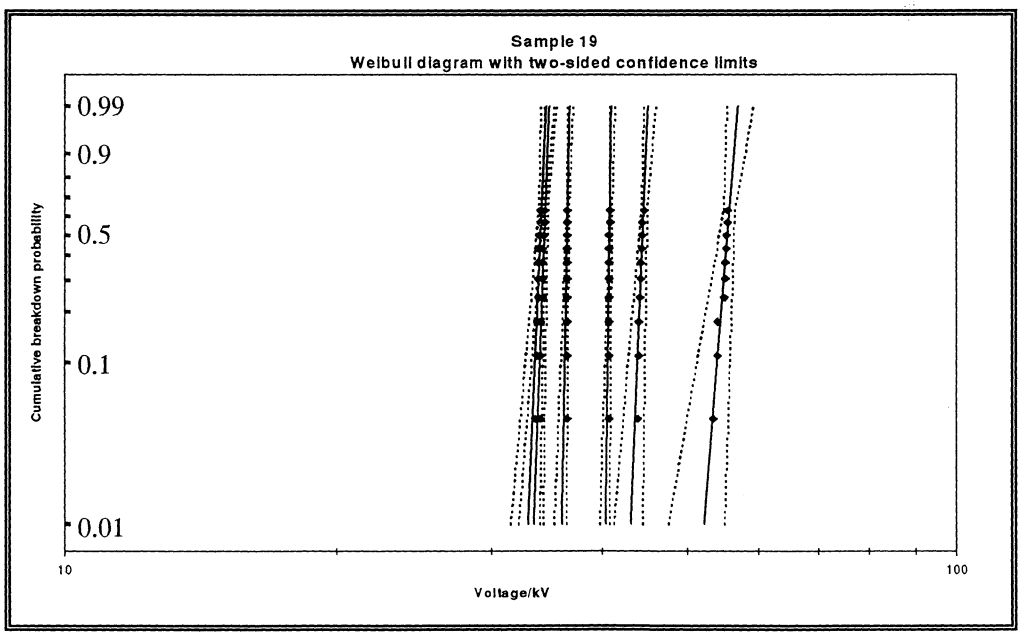

Figure 32. Weibull-diagram with confidence limits.

The confidence limits are however closely related to the Weibull exponent (steeper slope gives narrower limits) why no new differences between the samples are found this way.

4.5.2. Focus in front of (and behind) the Surface

By moving the focusing lens away from the electrodes the focus moved out from the sample. Plasma was still generated at the surface but the energy was distributed over a larger area. Figure 33. shows U_{50} as a function of pulse energy for sample 22 and 24 with the focus approximately 3 mm in front of the surface. Measurements were made with both positive and negative high-voltage on the electrode.

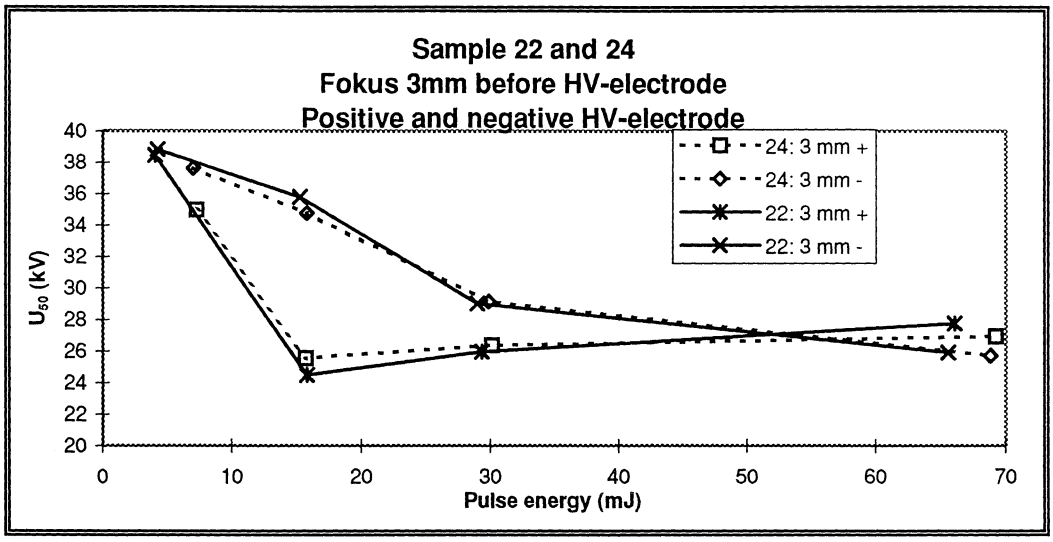

Figure 33. U_{50} versus pulse energy for both polarities.

Just as before no significant difference can be found between the samples. On the other hand it is clear that by moving the focus the U_{50} has dropped considerably. Another interesting phenomenon is the difference between the two polarities and the shapes of the curves.. This effect was therefore studied further.

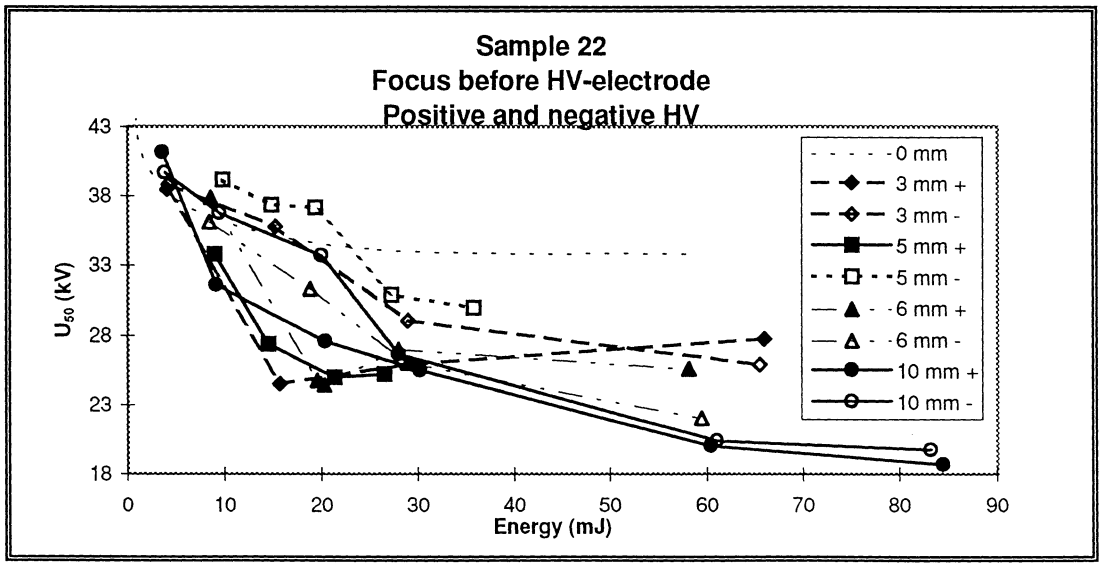

Figure 34. U_{50} versus pulse energy for both polarities and various positions of the focus.

Figure 34. show U_{50} plotted against pulse energy for different positions of the focus but only for sample 22. Of great interest here are the very low values of U_{50} and the gap between the values for positive and negative polarity.
Note that with the focus on the surface, the U_{50} never reached below 33 kV (Figure 29).

Figure 35 clearly shows what happens when the focus is moved out from the surface. As the position of the focus is moved away from the sample, the surface plasma shrinks and the volume plasma follows the focus. With the focus at more than 20 mm away the intensity at the surface is just enough to create a small plasma.

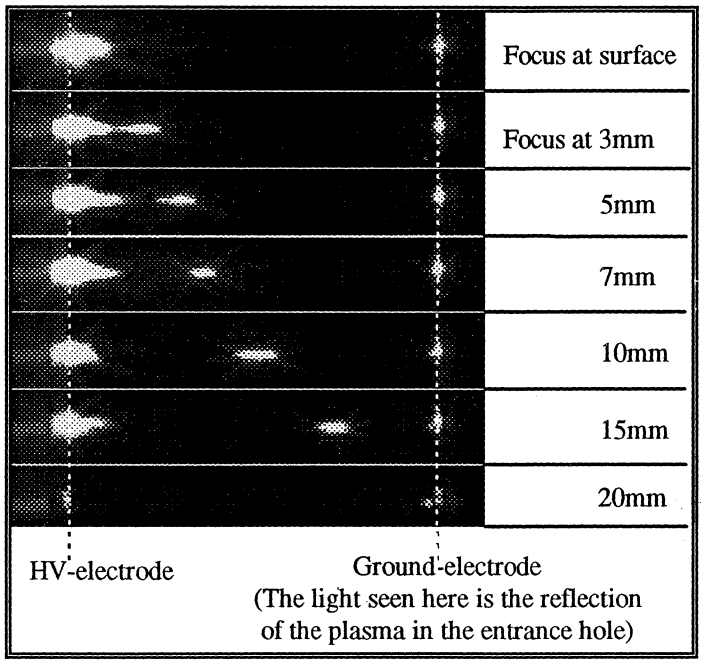

Figure 35. Plasma with various positions of the focus.

Figure 36 show the same thing but with a complete electrical breakdown as well. Here we can also observe indications of laser guiding of the discharge [8]. With the focus at the electrode surface the laser field in the middle of the gap is fairly weak (wide beam) thus not causing any ionisation. The breakdown arc thus propagates in a straight line to the nearest part of the ground electrode, i.e. the edge of the 20 mm hole (Ch. 4.3.1.2) through which the laser is directed. When the focus is moved out into the gap the ionisation there due to the laser field will increase. The streamer and consequently the breakdown arc, will therefore propagate easier in the path of the laser pulse, not deviating from it until it gets close to the ground electrode. Here it will make a sharp turn to reach the edge of the entrance hole.

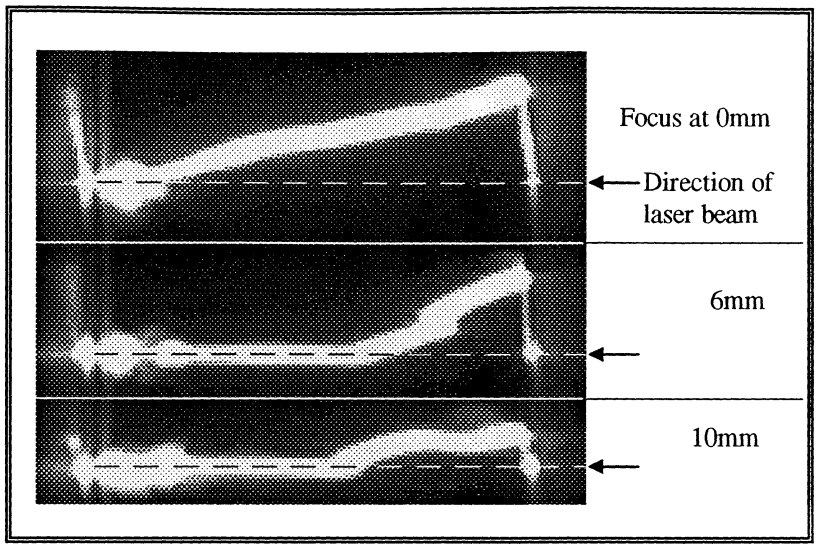

Figure 36. Breakdown with various positions of the focus.

The delay times from these measurements are assembled in Table 7 (Appendix C) together with some statistical calculations. The results are very irregular making them difficult to summarise and interpret. This is also why I include a large table instead of a diagram. Several interesting remarks can nevertheless be made about specific series:

- For a focus position of 5 mm the delay times go from short and rather stable for positive HV-electrode to very long and unstable for negative HV-electrode.
- The same can be said for a focus position of 6 mm although here the positive HV-electrode give long delay times for high energies.
- For a focus position of 10 mm the delay times are very long but stable.

The average for all delay times with positive HV-electrode is 60% of the average with negative HV-electrode.

A few measurements were also made with the focus moved inside the surface of the sample but this increased the voltage required for breakdown even above the original level so the method was discarded for the rest of the project.

The Weibull exponent was calculated and it varied between 50 and 450 although values above 300 and below 90 were very rare. No other generalisations could be made except that the exponent seemed slightly smaller than when the laser was focused at the surface. It must however be noted that for the focus-on-surface experiments, fifteen triggered breakdowns were made while for the focus-before-surface experiments only ten or even five (3 mm) were made. Figure 37 show the worst series in my experiments or the series giving the lowest Weibull exponent and the widest confidence limits.

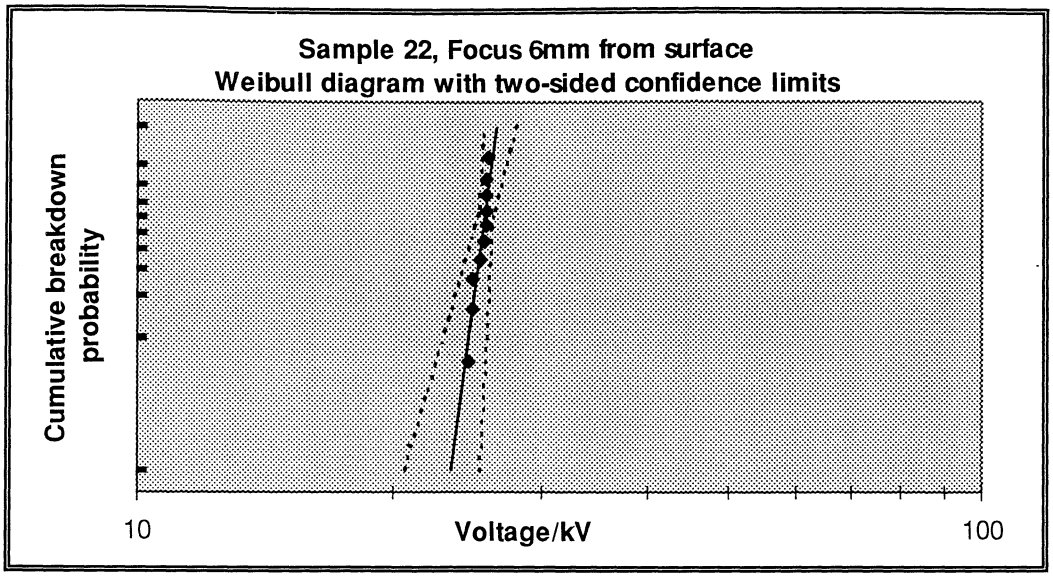

Figure 37. Weibull diagram with confidence limits, showing the "worst" of all series.

4.5.3. Laser Damage

Moving the sample in the electrode meant touching the rather unstable electrode set-up. To minimise the impact of this and to save time I decided to move the sample only after a proper breakdown and not after every laser pulse. This meant "shooting in the same hole" several times, causing extensive laser damage and thereby altering the surface structure. Experience show however that this did not affect my results. A few experiments moving the sample between every shot gave exactly the same results. I also tried setting the voltage slightly above the expected breakdown level and would then always get breakdown on the first shot, even on clean, undamaged surfaces.

5. Discussion

5.1. SURFACE TRIGGERING IN GENERAL

It is evident from figure 27 and figure 29 that laser triggering on the surface of the electrode is an effective way of controlling the electrical breakdown of a spark gap. Not only is the voltage at which breakdown will occur lowered considerably. The lower limit also seem to get more well defined. That is, the slope of the Weibull diagram is in most cases more than a factor two steeper for triggered breakdown than for spontaneous breakdown (Table 5), which is the same as saying that the confidence limits are narrowing by approximately the same amount. Finally, the triggering makes it possible to control the breakdown in time, down to a few nanoseconds, although I never saw delay times below 0.4 microseconds.

5.2. DIFFERENT SURFACES

The expected differences between the various samples were not seen. Considering the errors involved, the plotted points in figure 29 are extremely close together indicating a very strong relationship between U_{50} and pulse energy. Comparing with the enormous differences in delay times, suggesting completely different breakdown processes, make the results even more surprising.
The non-existence of a dependency of U_{50} to the absorptance or the roughness of the triggering surface should be due to one of the following reasons:

1) Absorption of laser energy at the surface of the electrode play an insignificant role in the triggering process.
2) Absorption of laser energy at the surface of the electrode play an important role in the triggering process but the difference in absorption is compensated by other phenomena thus making the net effect zero.

These could be explained in the following way:

1) Only a very small part of the laser energy is used to seed the creation of the plasma. Once the plasma is created, all remaining laser energy is absorbed by this and not by the electrode surface due to the fact that the plasma is completely opaque to the light [9]. Since all that is needed is this plasma seed, in my case requiring far less than a mJ of laser energy, the absorptance becomes unimportant. This does not however mean that there should be no difference in the minimum pulse energy required to create a plasma (Table 4).
   One thing arguing against this theory is the fact that the laser pulse leaves rather big marks on the surface. This could however maybe be explained by the heat of the plasma ($>10^4$ K). Energy is thus transferred from the laser pulse to the surface via the plasma. It has been shown [10, 11] that the plasma grows in a speed indicating significant interaction between the laser pulse and the plasma surface. Streak photos also show that

the plasma will reach considerable size during the duration of even a short (10 ns) laser pulse (Figure 38).

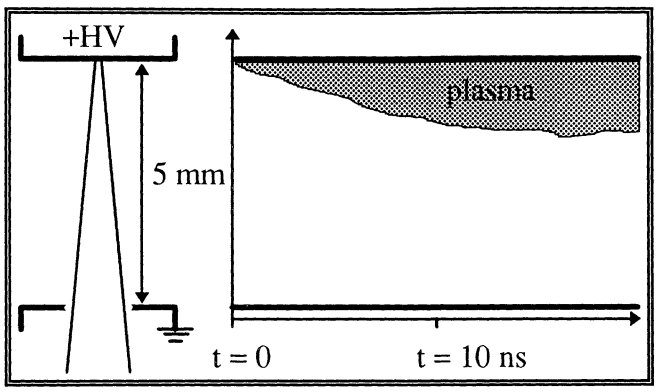

Figure 38. Sketch of streak photograph of plasma growth.
(t = 0 at laser pulse impact)

2) The pulse energy not absorbed by the surface is consequently reflected and therefore increase the laser field just outside the surface. This aids the growth of the plasma and compensate for the lack of energy absorption at the surface.

According to established theories [12] the delay time and the jitter is supposed to drop with increasing voltage. This is partly due to the fact that higher voltage means faster streamer propagation. If the streamer is fast enough it can even interact with the final parts of the laser pulse and thereby receive additional ionisation energy through inverse bremsstrahlung, leading to even shorter delay time and lower jitter. This is called laser guided streamer propagation. It can naturally only occur for delay times in the vicinity of the pulse length which however never was the case for me.
Several of my experiments gave delay times of over a hundred microseconds which is far more than the time it takes for ions to drift across the gap. It has therefore been suggested [13] that secondary emission induced by these ions could play a role here. This means that ions impacting on the cathode knock out several electrons creating new electron avalanches (chapter 4.1.1) that eventually cause the breakdown.
Throughout my experiments I measured the limits of triggered breakdown, why the voltage always was a function of the pulse energy. Being on the limit of triggered breakdown naturally increased delay times and jitter but it also led to opposing effects. An increase in pulse energy increases the amount of plasma in the gap. Intuitively an increasing amount of ions should aid the breakdown process and make it faster. On the other hand, increasing pulse energy lead to breakdown at a lower voltage (Figure 29) which means slower streamers, thus increasing the delay time.
To summarise it can be said that at the outer limits of triggered breakdown the delay times become fairly long but especially very unpredictable and unstable. At very high voltages though, the increasing speed of the streamers dominate giving shorter delay times and less jitter.

5.3. FOCUS POSITION

Moving the focus out from the surface dramatically changes the breakdown characteristics. The voltage required for breakdown is in many cases lowered by more than 25% (Figure 34).

This can maybe be explained with the first theory mentioned above:

Since only a little energy is needed to seed the creation of the plasma, having a focus a few millimetres outside the surface will further accelerate and concentrate the growth of the plasma. Moving the focus even further leads to the creation of a free secondary plasma in the gap (Figure 35 and 39). It is opaque to the laser light, thus casting it's shadow towards the HV-electrode surface, preventing the plasma there from further growth. Being highly conducting it however shortens the distance needed to be crossed by the streamer and also, by the allocation of charges in the plasma, increases the electric field in the gaps.

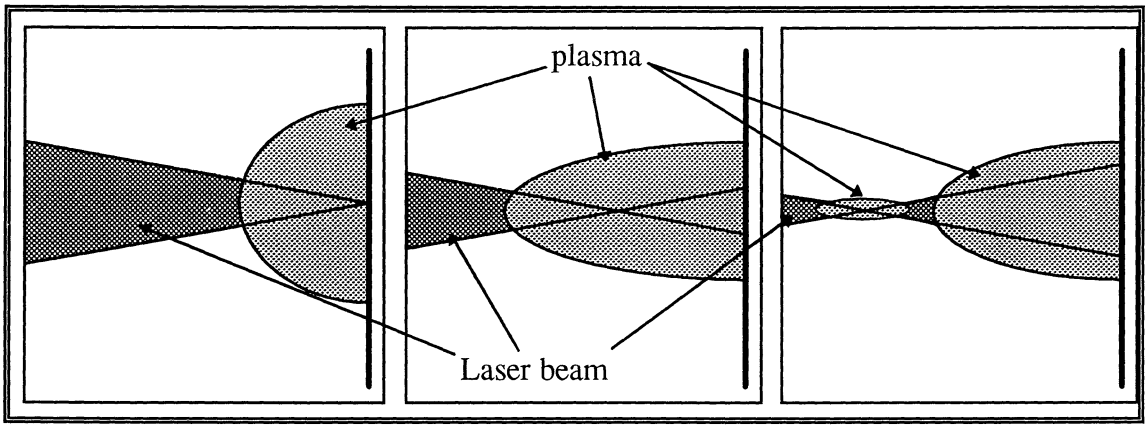

Figure 39. Plasma growth with different focus of the laser pulse (See also figure 35).

Several authors have mentioned differences in delay times when letting the laser pulse impinge on the anode or the cathode. It is however more difficult to find any explanations to the gap in the diagram (Figure 33) showing U_{50} versus pulse energy for different polarity of the HV-electrode.

5.4. CONCLUSION

Laser triggering on the surface of one of the electrodes is a very effective way of controlling the breakdown of a spark gap. Rather surprisingly, neither the absorptance of the laser wavelength nor the surface roughness, i.e. the surface structure on microscopic level, seem to have any impact on the breakdown process. The cause for this is probably that the direct absorption of laser light on the electrode surface is insignificant compared to the absorption of light in the plasma created by the laser.

The position of the focus has however a great impact on the breakdown characteristics. The voltage required for breakdown at a given laser energy is lowered considerably when moving the focus out from the surface. More work need to be done to investigate this phenomenon and to find the optimal position and length of the focus. The focal length of the focusing lens is probably of great importance since it not only changes the length of the focus in the gap but also the spot-size on the electrode. With a longer focal length the peak intensity at the surface can be kept high despite having moved the focus away from the electrode.

It is difficult to draw any general conclusions regarding the delay times since I throughout my experiments have stayed on the limit of breakdown where the jitter is substantial and where changing one parameter (pulse energy) means automatically changing the other (gap voltage). My results are however not contradictory to established theories concerning the relation between delay time and percentage of spontaneous breakdown-voltage [11].

More work also need to be done regarding the impact of changing the polarity of the electrode gap. Due to practical reasons I was only able to trigger on the high-voltage electrode. Would triggering on the ground electrode change the breakdown characteristics?

6. Appendix

Appendix A

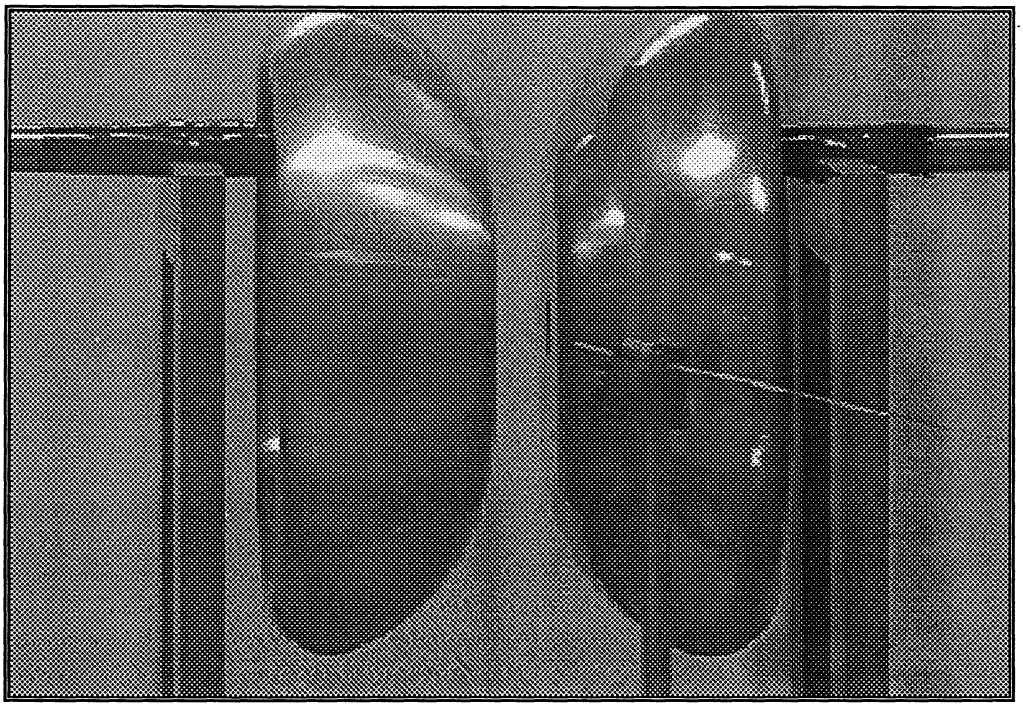

Figure 40. CCD-picture of the electrode gap. The left electrode is high-voltage and the right is ground. The entrance hole for the laser beam can bee seen in the middle of the ground electrode as a dark spot. Note also the optical fibre used for monitoring the delay times. The electrode diameter is 273 mm.

Appendix B

	Delay times																				
	Sample 5				Sample 8				Sample 19					Sample 22					Sample 24			
Energy (mJ)	70.0	32.0	15.0	4.6	55.0	23.0	9.3	2.4	58.0	23.0	9.2	2.4	0.88	58.0	26.0	9.1	2.4	0.69	58.0	24.0	9.2	2.3	0.77
Voltage (kV)	33.4	33.8	35.5	38.5	34.1	34.3	36.3	40.2	34.0	34.4	36.4	40.7	44.4	33.8	34.1	36.3	39.8	45.1	34.2	34.4	36.2	39.9	44.4
Delay times		3.96	2.8	1.65	195.5	65.3	3.36	2.96	3	32.8	99.6	1.3		12.8	105	35.9	1.2		51		171.6	1.21	1.16
(μs)			164.8	1.85	130.5		16.64	3.54	300		120	0.9	0.98	303	3.6	41.2	1	0.72	32	3.6			0.72
		2.7	28.4	7.96	38.5	202.4	12.56	1.26	8	168.6	6	1.1	0.9	54.8	35	179	1.1	0.93	15.8	4	94.6	1.14	0.7
		1.6	3.2	1.24	86.2	3.8	19.5	1.1	12.6	289	79.1	1.2	1.05	302	2.8	1.6	1	0.58	16.2	58.8	2.6	1.18	0.98
	129	4	319	1.3	15		4.24	1.48	36.4	89.6	2.96	1.4	0.54	67.2	63.8	166	1.1	0.49	40.4	4.8	107.6	1.33	0.66
	146		7	13	40.5	2.4	6.32	1.1	151	205	33.7	1.4	0.98	133	215	38.8	1.4	0.5	84.8	2	3	1.75	0.74
	131	1.6	5.6	1.15	12.5	6.24	67.12	1.1	299	129	2.64	1	0.67	145	130	86	1	0.72	107.8	131.4		1.05	0.72
			146.8	1.3	9.8	5.92	35	1.02	240	32.8	27.44	1	0.96	25	62.8	4.4	1.1	0.58	3.2	2.8	101.4	1.18	1.12
		9.6	65.6	1.68	130.2	2.72	51.2	0.98		88	59.3	1.3	1	170	167	19.8	1	0.74	14	2.6	4.8	1.58	0.64
				1.44	117.8	128.4	1.92	0.84	16.2	152	16.5	1.3	0.72	23.2	3	1.9	1.2	0.66	14.4	10.8	7.4	1.11	0.88
	227	51.6	2	2.66	14.6	134.5	2.48	1	53.4	3	151	1.05	0.98	25.4	129		1	0.57	50.6	79.4	61.4	1.01	0.52
	159	2.4	3	1.28	12.5	92.64	83.4	1.22	313	94.8	95.2	1.3	1	90	253	37.8	1.2	0.6	17.6	143.2	21.4	1.14	0.48
	63		6.5	1.5	5.5	12.6	15.9	0.96	3	2.2	47.9	1.5	0.72	64.4	2	47.6	1.2	0.65	2.2	2.8	29	1.16	
	32	149.2	13.2	1.55	36	33.8	144	0.96	2.2	36.8	114	1	0.78	296	54.8	33.2		0.63	8.8	2.4	128.4	3.07	0.6
		5		1.1	27.2	2.8	2.08	1.22	14.6	82.8	3.28	1	0.8		53	15.6	1.4	0.66	27.4	3	2.5	1.15	0.5
Median time	131	3.98	7	1.5	36	12.6	15.9	1.10	26.3	88.8	47.9	1.20	0.93	78.6	62.8	36.85	1.10	0.64	17.6	3.8	29	1.17	0.71
Average time	127	23.2	59.1	2.7	58.2	53.3	31.0	1.38	104	100	57.2	1.18	0.86	122	85.3	50.6	1.14	0.65	32.4	32.3	56.6	1.36	0.74
Standard dev.	63.93	46.81	95.98	3.317	59.05	66.33	40.3	0.78	127.7	82.07	49.51	0.19	0.16	107.7	79.54	56.2	0.14	0.11	30.4	50.52	57.93	0.53	0.22
Std.dev./Med	0.49	11.76	13.71	2.211	1.64	5.265	2.534	0.71	4.855	0.92	1.0	0.16	0.17	1.37	1.267	1.525	0.13	0.18	1.727	13.29	2.0	0.45	0.31

Table 6. Delay times.

Appendix C

		Delay times																
Positive	Focus (mm)	3	3	3	3	5	5	5	5	6	6	6	6	6	10	10	10	10
HV-electrode	Energy (mJ)	15.7	29.3	66	4.05	21.3	26.5	14.5	8.98	20.3	19.5	58.1	28	8.53	60.4	30.2	20.4	9.15
	Polarity	+	+	+	+	+	+	+	+	+	+	+	+	+	+	+	+	+
	Voltage (kV)	24.5	26	27.7	38.5	25	25.2	27.4	33.8	24.4	24.7	25.6	27	37.9	20	25.5	27.6	31.6
	Times (μs)	1.7	0.32	160	122	1.9	0.8	0.97	0.62	1.06	1.24	61	174	0.72	360	350	350	290
		0.56	0.48	190	1.2	0.92	0.98	0.62	1.1	2	0.81	60	198	0.65	270	330	440	220
		3.8	0.58	270	130	3	1.5	0.9	0.6	1.2	0.74	124	41	1.4	340	410	360	230
		3.6	0.44	180	140	1	0.92	0.86	0.62	2	3.8	190	69	0.75	400	360	310	300
		0.4	0.44		1.44	1.2	0.86	0.8	6	1.1	0.9	47	88	1.5	310	360	290	280
						0.8	0.82	0.74	0.64	1.1	1	140	59	1.5	430	330	310	255
						1	0.72	0.74	0.54	1	1.2	95	59	0.71	370	345	390	280
						0.86	0.78	0.68	0.48	1.1	1.1	74	57	0.9	390	360	400	250
						0.68	0.74	0.66	0.5	0.84	1.1	53	41	1.2	430	330	460	220
						0.98	0.8	1.2	0.82	1.2	1	34		1.5	410	340	320	270
	Median	1.7	0.44	185	122	0.99	0.81	0.77	0.62	1.1	1.05	67.5	59	1.05	380	348	355	263
	Average	2.01	0.45	200	78.9	1.23	0.89	0.82	1.19	1.26	1.29	87.8	87.3	1.08	371	352	363	260
	Std.dev.	1.62	0.09	48.3	71.1	0.7	0.23	0.17	1.7	0.4	0.9	49.4	58	0.37	52.4	24	58.1	29.1
	Std.dev./med.	0.95	0.21	0.26	0.58	0.71	0.28	0.23	2.74	0.37	0.85	0.73	0.98	0.35	0.14	0.07	0.16	0.11
Negative	Focus (mm)	3	3	3	3	5	5	5	5	5	6	6	6	6	10	10	10	10
HV-electrode	Energy (mJ)	65.5	29	15.2	4.22	35.7	27.2	14.9	19.3	9.82	59.4	28.9	18.8	8.44	61.1	28	20	9.47
	Polarity	-	-	-	-	-	-	-	-	-	-	-	-	-	-	-	-	-
	Voltage (kV)	25.9	29	35.8	38.8	30	30.9	37.4	37.2	39.2	22	26	31.3	36.1	20.4	26.6	33.7	36.8
	Times (μs)	7.2	180	4.6	210	259	170	173	8	223	22	141	8.4	220	300	350	450	260
		6.8	250	8.4	170	355	392	8.6	10	218	18	155	6.5	260	300	270	220	450
		5.8	27	8.8	210	263	7	10	10.2	119	170	150	5	200	180	106	440	330
		6.5		3.1	180	361	261	10.4	9.4	237	170	145	5.8	280	200	150	500	260
		5.1		9		165	211	10.2	9.8	13	150	163	4.6	270	260	250	550	390
						375		9.2	9.2	122	150	127	4.3	255	290	140	710	370
						178		225	183	158	25	155	3.7	300	330	170	620	310
						332		11.6	189	101	170	144	4.5	265	220	290	510	350
						309		8.6	1.6	153	150	140	4.3	260	160	220	550	240
						215			8.4	255	140	147			340	250	690	350
	Median	6.5	180	8.4	195	286	211	10.2	9.6	156	150	146	4.6	260	275	235	530	340
	Average	6.28	152	6.78	193	281	208	51.8	43.9	160	117	147	5.23	257	258	220	524	331
	Std.dev.	0.83	114	2.74	20.6	77	140	84.4	75	74.9	66.3	9.94	1.46	30.1	64.1	76.7	141	65.6
	Std.dev./med.	0.13	0.63	0.33	0.11	0.27	0.66	8.28	7.81	0.48	0.44	0.07	0.32	0.12	0.23	0.33	0.27	0.19

Table 7. Delay times with various position of the focus.

7. Acknowledgements

I would like to thank my supervisor Anders Sunesson and my examiner Stefan Kröll both at the Department of Physics in Lund and Mikael Bergkvist at ABB Corporate Research, for assisting me with this work. Finally I would like to thank Per Nostell and the others at the Department of Solid State Physics in Uppsala for their assistance and friendliness during and after my stay there.

8. References

1.	W.K. Pendleton & A.H. Guenther,	Investigation of a Laser Triggered Spark gap, Rev. Sci. Inst.., 36:62 (1965)
2.	J.R. Woodworth, R.G. Adams & C.A. Frost	UV-Laser Triggering of 2.8-Megavolt Gas Switches, IEEE Trans. On Plasma Sci., PS-10, no 4:257 (1982)
3.	M. Adomat	Laser Triggered Spark Gaps, ABB Corporate Research, SECRC/H/TR-96/156E (1996)
4.	H.E. Bennett & J.O. Porteus	J. Opt. Soc. Am. 51:123 (1961)
5.	J.M. Bennett & L. Mattsson	Introduction to Surface Roughness and Scattering, UUIP-1185, p 51, Uppsala, (1988)
6.	J. Garmer	Laser Shadow Imaging of Laser-initiated Electric Prebreakdown Events in Transformer Oil, LRAP-199, Lund (1996)
7.	W. Hauschield & W. Mosch	Statistical Techniques for High-Voltage Engineering, Peter Peregrinus Ltd, London (1992)
8.	M. Miki, Y. Aihara & T. Shindo	Development of Long Gap Discharges Guided by a Pulsed CO_2 Laser, J. Phys D: Appl. Phys. 26:1244-1252 (1993)
9.	F.F. Chen	Introduction to Plasma Physics and Controlled Fusion, Plenum Press, N.Y. (1984)
10.	R.A. Dougal	Breakdown Processes in Laser Triggered Switching, Texas Tech. Univ. (1983)
11.	R.A. Dougal & P.F. Williams	Fundamental Processes in the Laser-Triggered Electrical Breakdown of Gases, J. Phys. D., 17:903 (1984)
12.	A.H. Guenther & J.R. Bettis	Laser Triggered Megavolt Switching, IEEE J. Quantum Elect., QE-3:581 (1967)
13.	P.F. Williams & A.H. Guenther	Laser Triggering of Gas Filled Spark Gaps, Gas Discharge Closing Switches, Plenum Press, N.Y. (1990)